Damage control in the plant kingdom: a case study on the morphology, anatomy, and biomechanics of the European mistletoe (*Viscum album*) and selected cacti species

Inaugural-Dissertation
zur Erlangung der Doktorwürde
der Fakultät für Biologie
der Albert-Ludwigs-Universität Freiburg im Breisgau

vorgelegt von
Max David Mylo
geboren in Kehl-Kork

Freiburg im Breisgau
Mai 2022

Datum der Promotionsprüfung: 21. Oktober 2022

Diese Arbeit wurde angefertigt unter der Leitung von

Prof. Dr. Thomas Speck

an der

Albert-Ludwigs-Universität Freiburg
Fakultät für Biologie
Botanischer Garten und Plant Biomechanics Group Freiburg
Schänzlestraße 1
79104 Freiburg i. Br.

Max D. Mylo: Damage control in the plant kingdom: a case study on the morphology, anatomy, and biomechanics of the European mistletoe (*Viscum album*) and selected cacti species; Mai 2022.

Dekanin der Fakultät für Biologie:
Prof. Dr. Sonja-Verena Albers

Promotionsvorsitzender:
Prof. Dr. Andreas Hiltbrunner

Stellvertretender Promotionsvorsitzender:
Prof. Dr. Wolfgang Schamel

Referent & Betreuer der Arbeit:
Prof. Dr. Thomas Speck

Korreferent*in:

Drittprüfer*in:

Datum der mündlichen Prüfung:

für Oma & Opa

DANKSAGUNG

Ich möchte mich an dieser Stelle ganz herzlichst bei allen bedanken, die mich in den letzten Jahren hinweg unterstützt haben. An erster Stelle geht mein Dank an meinen Doktorvater Prof. Dr. Thomas Speck und an meine Betreuerin Dr. Olga Speck, die mir ermöglicht haben diese Arbeit in ihrer Arbeitsgruppe zu schreiben, die sich all meinen Fragen angenommen haben, mit wertvollen Tipps und Korrekturen zu erfolgreichen Messreihen und den daraus folgenden Publikationen beigetragen haben, und die auch sonst immer ein offenes Ohr für mich hatten.

Dr. Tom Masselter und Dr. Linnea Hesse möchte ich für ihre Zeit und weitergegebene Expertise, speziell zur 3D-Bildgebung, zu Beginn des Projektes bedanken. Unseren Kooperationspartnern Prof. Dr. Frank Balle und Samuel Beisel vom INATECH Freiburg danke ich für den reibungslosen Wissensaustausch und die Bereitstellung des Digitalmikroskops samt Einführung zur quantitativen Bruchflächenanalyse und für die Hilfestellung bei der Auswertung der Daten. Dem Team der Werkstoffprüftechnik der Universität Dortmund um Prof. Dr. Frank Walther und Ronja Scholz möchte ich für die Unterstützung bei der Visualisierung der endophytischen Mistel-Strukturen und der gemeinsamen Publikation danken. Bei Prof. Dr. Siegfried Fink und Dr. Kathrin Drozella möchte ich mich für die Sequenzierung der Opuntien und besonders für die Geduld mit den schier unmöglichen Dünnschnitten von *Cylindropuntia bigelovii* bedanken.

Ein ganz besonderer Dank geht an Friederike Krüger und Mara Hofmann, die im Zuge dieses Projektes ihre Masterarbeiten geschrieben haben und ihre Projekte mit viel Selbstständigkeit, Fleiß, Ausdauer und cleveren Ideen gefüllt haben. Auch bei Mark Kelbel und Daniela Neugebauer möchte ich mich für ihre zuverlässige Mitarbeit als studentische Hilfskräfte bedanken.

Mein Dank gilt der gesamten Plant Biomechanics Group, dem botanischen Garten der Universität Freiburg, dem Team der Arbeitsgruppe Technik der Biologie II/III um Dirk Renz und Jürgen Schmidt und der Projektleitung und -verwaltung des Exzellenzclusters *liv*MatS. Theresa Jones möchte ich für ihre unermüdliche Hilfe zur Verbesserung meines Englisch in den publizierten Arbeiten und dieser Thesis danken. Ein besonderer Dank geht dabei

an Sandra Caliaro für ihre Offenheit und Hilfe bei allem was das Labor betrifft und vielem darüber hinaus, an Martina Goldmann an die man sich mit jeder Frage wenden kann und an Dirk Rohleder und sein Gärtner*innen-Team, die die letzten Jahre geholfen haben meine stachligen Untersuchungsobjekte bei Wasser zu halten. Bei Dr. Falk Tauber und Max Langer möchte ich mich zunächst für die Verführung zum gesteigerten Kaffeekonsum entschuldigen und mich aber vor allem herzlichst bei euch beiden für die Zeit als beste Büro-Gemeinschaft bedanken!

Neben all den genannten Personen die einen direkten Anteil an dieser Arbeit haben, möchte ich mich besonders bei denen bedanken, die mir während dieser Zeit zur Seite standen und geholfen haben meinen Alltag abwechslungsreich zu gestalten. Dieser Dank gebührt meiner Familie, all meinen fantastischen Freunden, meiner Handball-Truppe und natürlich meiner wundervollen Partnerin Johanna. Danke für die tolle Zeit und ich freue mich auf all das was uns erwartet!

TABLE OF CONTENTS

VORWORT

Die vorliegende Dissertation wurde in kumulativer Form im Rahmen des Exzellenzclusters *Living, Adaptive and Energy-autonomous Materials Systems* (kurz *liv*MatS) angefertigt, das durch Fördermittel der DFG finanziert wird. Die vorgestellte Arbeit ist dabei Teil des interdisziplinären Forschungsbereichs C, in dem Chemiker*innen, Werkstofftechniker*innen, Mechaniker*innen und Biologen*innen gemeinsam nach Mechanismen suchen, die in Zukunft zur Langlebigkeit von neuartigen, bioinspirierten Materialsystemen beitragen. Dabei ist es die Aufgabe der Biologinnen und Biologen passende Mechanismen der Schadensvermeidung, der Selbstreparatur und der Fehlertoleranz in pflanzlichen Systemen zu untersuchen und diese auf ihr Potential hinsichtlich der Steigerung von Langlebigkeit, Stabilität und Widerstandsfähigkeit von Materialsystemen zu prüfen. Zusätzlich sollen im Austausch mit den anderen Fachrichtungen Möglichkeiten zur Übertragung von den biologischen Vorbildern auf die technischen Materialsysteme herausgearbeitet und in ersten Demonstratoren realisierbar werden.

Diese Arbeit behandelt die Analysen der Schadensvermeidung an der Europäischen Mistel (*Viscum album*) und ihrem Wirt, Selbstreparatur- und Abszissionsanalysen an ausgewählten Arten der Kakteen (*Opuntia ficus-indica* und *Cylindropuntia bigelovii*), sowie einen Artikel der das Themenfeld der pflanzen-inspirierten Schadenskontrolle bezüglich ihres Potentials zum Beitrag von langlebigen, bioinspirierten Materialsystemen im Zeitalters des Anthropozäns einordnet. In **Kapitel I**, dem Rahmen dieser Arbeit, werden die Ziele der Arbeit formuliert, der aktuelle Stand der Forschung in einer Einleitung beschrieben, die wichtigsten genutzten Methoden vorgestellt und die Hauptergebnisse präsentiert und diskutiert. **Kapitel II**, der Hauptteil dieser Arbeit, umfasst fünf wissenschaftliche Artikel und ein Manuskript, die im Rahmen dieser Arbeit im Peer-Review Verfahren publiziert wurden oder deren Einreichung bevorsteht. Zu jeder dieser Publikationen finden sich zudem Angaben zu dem von mir und den anderen Autor*innen daran geleisteten Anteil. Das letzte **Kapitel III** umfasst alle von mir im Zeitraum dieser Arbeit verfassten Publikationen, Konferenzbeiträge und Jahresberichte, sowie die (mit-)betreuten studentischen Abschlussarbeiten.

Part I

FRAMEWORK OF THIS STUDY

The framework of this study consists of six chapters. The first chapter comprises the objective of this work and an abstract in both German and English. The second chapter briefly introduces the concept of damage control and the biological background of the plant models investigated. The main methods used to collect the data are described in the third chapter. The fourth chapter presents and discusses the main results. This is followed by a conclusion and an outlook of the study. A list of the referenced literature is given in the last chapter of the framework.

1 OBJECTIVES AND ABSTRACT

1.1 Objectives

This work was conducted as part of the interdisciplinary project Living, Adaptive and Energy-autonomous Materials Systems (*liv*MatS). The overall goal of this project is to develop life-like material systems inspired by nature. These systems will be able to absorb clean energy from their environment (research area A), adapt autonomously to the given environmental conditions (research area B), and have high longevity (research area C). In addition, they will be tested for their sustainability and social and ethical acceptance (research area D). The demonstrator team will then combine the results of the research areas with the aim of implementing them in 3D-printed demonstrators. The presented work is part of research area C and focuses on identifying suitable biological role-models for bioinspired approaches that will benefit the longevity of materials systems and on characterizing the underlying structural and mechanical mechanisms and properties. The links to research areas B and D will show the connections between the different fields of research as envisaged in the project.

A crucial aspect for the longevity of materials systems is 'damage control'. This includes a more efficient and sustainable use of material resources through concepts for proactive 'damage prevention' and through the development of concepts for the adequate handling of existing damage ('damage management'). In the context of this work, the hemiparasitic European mistletoe (*Viscum album*) and its multifunctional and life-long connection to the host was identified as a suitable biological model for damage prevention analyses. The goal of the studies on the interface between the mistletoe and its host was to analyze the morphological, anatomical, and biomechanical adaptations during joint development and, at the same time, the competitive growth of the two species. The branches of two selected cacti species (*Opuntia ficus-indica* and *Cylindropuntia bigelovii*) were selected for damage management analysis. Comparative morphological, anatomical, and biomechanical analyses were performed on the self-repair ability of the cacti after artificial wounding and on the abscission behavior of their lateral branches, both crucial concepts for dealing with damaged or no longer needed organs.

1.2 Zusammenfassung

Die Europäische Mistel (*Viscum album*) ist der wohl bekannteste und auffälligste pflanzliche Parasit in Mitteleuropa. Als immergrüner Hemiparasit geht sie eine strukturelle und funktionelle Verbindung mit ihrem Wirt ein und nimmt mit Hilfe des Haustoriums Wasser und gelöste Salze auf. Trotz der Größe von über 2 Metern und der daraus resultierenden zusätzlichen Gewichts- und Windbelastung ist ein mechanisches Versagen der Anbindung bisher nicht beschrieben. Mikrotomografische Aufnahmen an Mistel-Wirtsproben ergaben, dass das Haustorium im Laufe des gemeinsamen und gleichzeitig konkurrierenden Wachstums mit dem Wirt (> 20 Jahre) einen Formwandel durchläuft, bei dem sich die vielen kleinen Senker der jungen Mistel allmählich zu einem großen Senker vereinigen. Zelluläre und biochemische Gradienten glätten den mechanischen Übergang vom verholzten Wirtsgewebe zum unverholzten inneren Teil des Haustoriums. Zugversuche zeigten, dass mit zunehmendem Alter der Mistel die Zugfestigkeit konstant bleibt, obwohl ihre Maximalkraft zunimmt. Die hohe Schadenstoleranz der Verbindung wird zudem durch die Redundanz mehrerer Senker begünstigt, die in den Kraft-Weg-Kurven durch Vor- und Nachversagen sichtbar sind.

Opuntioideae sind die zweitgrößte Unterfamilie der Kakteen und bekannt für ihre charakteristische Wuchsform mit verketteten Ästen und ihre Fähigkeit, Wasser zu speichern. Vergleichende Selbstreparaturexperimente an Ästen von *Opuntia ficus-indica* und *Cylindropuntia bigelovii* zeigten, dass nach einer Verletzung der Fokus auf der Vermeidung von Wasserverlusten durch die Bildung von Wundperiderm liegt. Aufgrund ihrer zerbrechlichen Anbindung fällt die mechanische Heilung jedoch sehr gering aus, und es gilt das Konzept "ausreichend ist gut genug". Analysen der Ast-Ast Verbindungen der beiden Arten und ihrer wichtigsten mechanischen Gewebe ergaben, dass die lateralen Äste von *C. bigelovii* leicht abfallen, was der vegetativen Vermehrung dient. Die Verzweigungen von *O. ficus-indica* werden bereits in frühen Stadien durch Wachstum, die Auflagerung von versteifendem Periderm und Gefäßbündeln mit deutlich höherer Steifigkeit und Reißfestigkeit stabilisiert, was ihr baumartiges Wachstum und ihre vorwiegend sexuelle Fortpflanzung begünstigt. Die Ergebnisse der vorliegenden Dissertation zeigen, dass die analysierten Pflanzenmodelle und ihre Konzepte zur Schadensvermeidung und -bewältigung perfekte Inspirationsquellen für bioinspirierte Materialsysteme mit hoher Langlebigkeit darstellen.

1.3 Abstract

The European mistletoe (*Viscum album*) is probably the best-known and most conspicuous plant parasite in Central Europe. As an evergreen hemiparasite, it forms a structural and functional connection with its host, absorbing water and dissolved salts with the help of the haustorium. Despite its maximum size of more than 2 meters and the resulting additional weight and wind loads experienced by the host, the mechanical failure of the interface has never been described. Microtomographic scans of mistletoe-host samples have revealed that the haustorium undergoes a structural change during the development of the joint and the simultaneous competitive growth with the host (> 20 years), with the several small sinkers of the young mistletoe gradually merging together to form a larger main sinker. Cellular and biochemical gradients smoothen the mechanical transition from the lignified host tissue to the un-lignified inner part of the haustorium. Tensile tests have shown that, with the increasing age of the mistletoe, the tensile strength remains constant, although its maximum force increases. The high damage tolerance of the connection is furthermore facilitated by the redundancy of the individual sinkers, as is visible in the force-displacement curves through pre- and post-failure events.

The Opuntioideae are the second largest subfamily of cacti and are known for their characteristic growth habit with interlinked branches and their ability to store water. Comparative morphological, anatomical, and biomechanical self-repair experiments on branches of *Opuntia ficus-indica* and *Cylindropuntia bigelovii* have shown that, after injury, the focus is on preventing water loss through the formation of wound periderm. However, because of its fragile attachment, mechanical healing turns out to be very low, and the concept of 'sufficient is good enough' applies. Analyses of the branch-branch junctions of the two species and their main mechanical tissues have revealed an abscission behavior of the lateral branches in *C. bigelovii*, a feature that serves vegetative propagation. The junctions of *O. ficus-indica* are stabilized at early stages by growth, the deposition of a stiffening periderm, and vascular bundles with markedly higher stiffness and strength, all favoring their tree-like growth and, primarily, sexual reproduction. The outcomes of the work presented in this dissertation demonstrate that the analyzed plant models and their concepts of damage avoidance and management provide an excellent basis for bioinspired materials systems with high longevity.

2 INTRODUCTION

2.1 Damage control in plants

Injury and damage are omnipresent risks for plant and animal life. Unlike most animals, however, plants have no ability to flee from potential threats, such as predators, rockfall, or severe weather events (e.g., storm, fire, snow). Because of their spatial constraints, great evolutionary pressure has been brought to bear on terrestrial plants regarding the development of mechanisms that can best protect them against damage and enable them adequately to cope with existing damage. Together with the size of the threats, from microbes and spores (BAKER *et al.*, 1997) to mammals (BRYANT *et al.*, 1991) and large rocks (WIECZOREK, 2002), the hierarchical levels of protective mechanisms, from phytochemicals (BEDNAREK & OSBOURN, 2009) to the transformation or shedding of entire organs (ADDICOTT, 1982), also span multiple orders of magnitude.

In addition to damage caused by biotic factors (DANGL & JONES, 2001; which will only play a minor role in this thesis), failures occur when mechanical stresses exceed the ultimate strength of the tissues involved. Such stresses do not necessarily originate from external forces; they also occur during growth processes that can lead to internal fissures (GRIL *et al.*, 2017). In order to reduce and deal with these stresses, plants have developed a wide variety of adaptations that we can divide into 'damage prevention' and 'damage management' concepts, both of which can be subsumed under the umbrella term of 'damage control' (**Figure 1** and **Article B**).

Damage caused by strong wind or other abiotic forces mostly occurs at sites with marked geometric transitions or tapers or at sites at which the mechanical properties of the tissues involved undergo an abrupt change (NIKLAS, 1992). Damage prevention includes mechanisms that smoothen these transitions at a structural or mechanical level ('gradient structures') and mechanisms that help the plant to acclimatize or adapt to changing environmental conditions ('responsive structures'). However, if these measures are not sufficient, and if tissue damage occurs, damage management mechanisms can take effect that either repair structural damage ('self-repair') or discard the entire affected organ ('abscission') (**Figure 1**). A detailed description of the named concepts for damage control in plants and the way in which we can use them as the inspiration for sustainable solutions in the era of the Anthropocene are described in **Article B**.

2.1.1 Damage prevention in plants

Based on the highly hierarchical structure of plants, various gradual transitions of geometries and mechanical properties of tissues have emerged during their evolution to prevent overcritical local stress concentrations. Functional gradients can be achieved by various chemical compositions and/or by structural characteristics such as the arrangement, distribution, or orientation of tissues (LIU *et al.*, 2017). In addition, they can occur at interfaces of biological composites (STUDART *et al.*, 2014) and, as in the case of bamboo (WEGST *et al.*, 2015) and coconut (GRAUPNER *et al.*, 2017; SCHMIER *et al.*, 2020a; SCHMIER *et al.*, 2020b), encompass various hierarchical levels to increase the rigidity and strength of the material. Gradients at the levels of geometry, shape, size, and tissue arrangement are also found between the petiole and lamina of foliage leaves, providing a damage-resistant transition zone (LANGER *et al.*, 2021).

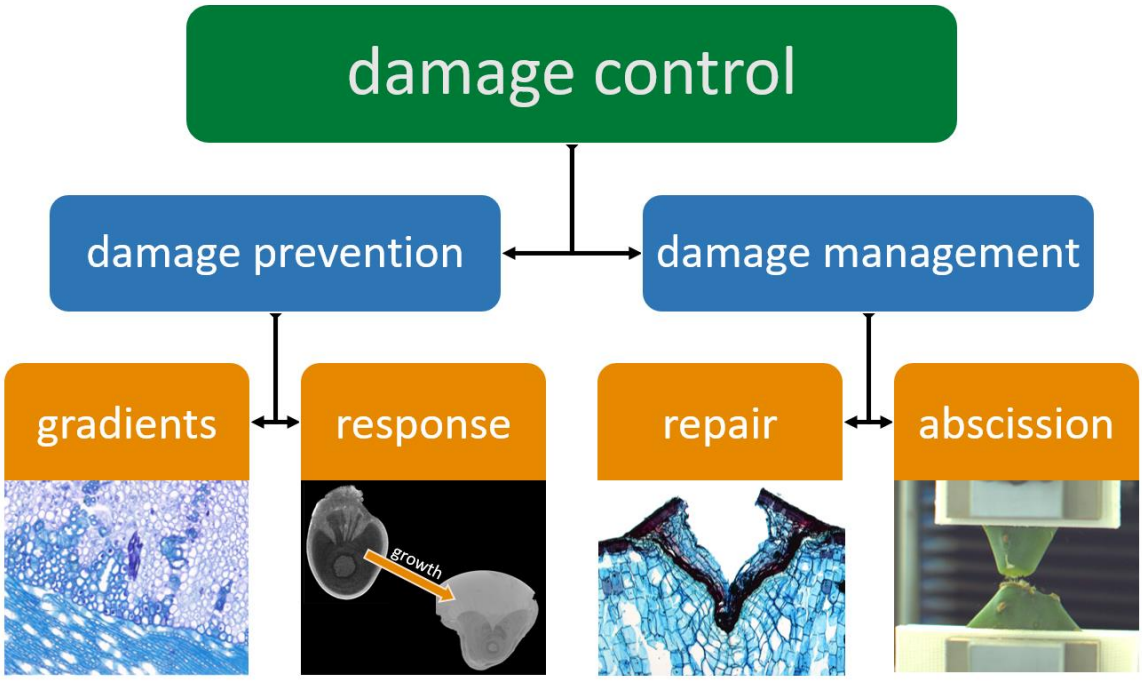

Figure 1: Damage control and the hierarchy of its subcategories damage prevention and damage management including selected examples from the plant kingdom described in the following chapters of this thesis. The concept is adapted from **Article B**, in which further details and examples of all categories can be found.

A further concept enabling plants to avoid damage is to respond to changing environmental conditions. A distinction is made between the reconfiguration of plants organs as an immediate response to external stimuli (e.g. leaves under wind load; VOGEL, 1989; TELEWSKI, 2021), the acclimatization to changing conditions during the life cycle of the plant

(e.g., within weeks to months in response to persistent or recurrent mechanical loading on organs; JAFFE, 1973; TELEWSKI & JAFFE, 1986; BADEL *et al*., 2015; LANGER *et al*., 2022), and the evolutionary adaptation within a population of plants over several generations through genetic recombination and selection (LAMBERS *et al*., 2008; LEIMU & FISCHER, 2008).

2.1.2 Parasitic plants

Plant parasites (from the Ancient Greek παρά (pará) meaning 'from' or 'beside', and σῖτος (sîtos) meaning 'grain' or 'food') are characterized by their structural and physiological connection to a host from which they draw water, dissolved salts, and, in some species, organic carbon (HEIDE-JØRGENSEN, 2008). Their ability to maintain this structural and physiological connection, while being constantly challenged to respond to changing conditions because of joint development and competitive growth with their host, makes them highly promising model organisms for damage prevention analyses.

Parasitic plants comprise over 4,500 species distributed over about 290 genera and 20 families and make up more than 1% of all flowering plants worldwide (WESTWOOD *et al*., 2010; NICKRENT, 2020; TEIXEIRA-COSTA & DAVIS, 2021), with their classification as parasites and their phylogeny being under constant debate during recent years (WESTWOOD *et al*., 2010; BROMHAM *et al*., 2013; NAUMANN *et al*., 2013; SU *et al*., 2015; TĚŠITEL, 2016; TWYFORD 2018).

Parasitic plants do not represent a monophyletic group but have evolved independently in twelve lineages (NICKRENT, 2020; TEIXEIRA-COSTA, 2021). They can be categorized by their photosynthetic ability to synthesize carbohydrates: More than 90% of plant parasites, the so-called 'hemiparasites', are photosynthetically active and rely only on water and dissolved salts from their host. This photoautotrophy is reflected by their (at least partially) green appearance because of the presence of chlorophyll. The other about 390 species, the so-called 'holoparasites', do not have the ability to photosynthesize and deprive their host of additional organic carbon (HEIDE-JØRGENSEN, 2008). Another distinguishing feature is the parasitized host organ, with a distinction between branch and root parasites (HEIDE-JØRGENSEN, 2008). Many root parasites, with their below-ground connections to the host and a reduced exophyte (the part of the parasite that grows outside the host; usually branches and flowers), are rarely visible to the common observer (MAUSETH & REZAEI, 2013; NIKOLOV *et al*., 2014; TEIXEIRA-COSTA *et al*., 2021). Branch parasites form their structural and functional connection with the host branch and, like the European mistletoe, can form a readily visible

part of our vegetation (WATSON, 2001; AUKEMA, 2003; TEIXEIRA-COSTA, 2021; **Figure 2**). They are often mistaken for epiphytes or for climbing and strangler plants, which also grow on (or around) other plants to secure an edge in the competition for sunlight by gaining altitude, but which do not form a physiological connection with the plant providing them with support and are therefore not classified as parasites (ATHREYA, 1999; ZOTZ & HIETZ, 2001; ROWE *et al*., 2004).

Figure 2: Trees heavily parasitized by the evergreen European mistletoe (*Viscum album* subsp. *album*) during winter time in southern Germany.

Plant parasites come in a wide variety of growth forms, from small herbs to trees (HEIDE-JØRGENSEN, 2008; TEIXEIRA-COSTA & DAVIS, 2021), but the feature that unites them all is the formation of a haustorium, an organ described by KUIJT (1969) as the 'very essence of plant parasitism'. The haustorium initially attaches to the host by means of appendages providing mechanical anchorage (such as the adhesive disc of the European mistletoe) and penetrates the dermal host tissues with so-called sinkers, with cell-wall-degrading enzymes being involved in at least some species (NAGAR *et al*., 1984; LOSNER-GOSHEN *et al*., 1998; OUYANG *et al*., 2016). These sinkers initially consist of parenchymatous cells that partially differentiate into tracheary elements or other conductive cells in later stages, thereby establishing a vascular connection with the host (TEIXEIRA-COSTA, 2021). During this process,

all parasites attach to the host xylem (forming a so-called xylem bridge), with only some developing an additional physiological connection to the host phloem, through which they can take up organic carbons (HEIDE-JØRGENSEN, 2008; TEIXEIRA-COSTA, 2021). In addition to the tissues involved in the transfer of nutrients, the haustorium can produce tissues that spread the parasite throughout the bark or wood of the host (mistletoes form so-called cortical strands that expand through the host cortex and from which adventive shoots can emerge) (CONDON & KUIJT, 1994). Together, all of these tissues growing inside the host form the endophyte of the parasite.

In addition to the functions of initial anchorage, the exchange of water, mineral salts, and genetic information (JOEL, 2013; YOSHIDA *et al*., 2016), and the spread within the host, the haustorium serves mechanically to anchor the parasite in the host tissue throughout its lifetime, making it a truly unique multifunctional organ (YOSHIDA *et al*., 2016).

2.1.2.1 The European mistletoe (*Viscum album*)

The genus *Viscum* belongs to the family of Santalaceae and comprises about 100 mistletoe species. Mistletoes are evergreen hemiparasites that grow on shrubs or trees and are mostly pollinated by insects (AUKEMA, 2003; STANTON *et al*., 2009). The most prominent and widespread mistletoe species in Central Europe is the European mistletoe (*Viscum album*), with its natural habitat extending to southwest Asia. Depending on the host species, four subspecies can be distinguished, with *V. album* subsp. *album* growing exclusively on dicotyledonous trees and being the most common subspecies in Germany (ZUBER, 2004). The other subspecies are *abietis* growing on *Abies* spp., *V. album* subsp. *austriacum* mainly parasitizing *Pinus* spp., and *V. album* subsp. *creticum* only growing on trees of *Pinus halepensis* subsp. *Brutia* on Crete.

Plants of *V. album* are dioecious, and the adult female mistletoes produce white berries. These are eaten by birds such as the mistle thrush (*Turdus viscivorus*), which spread the seeds by excretion (BECKER, 1986; VARGA *et al*., 2014). With the help of the highly sticky viscin of the exocarp (ZUBER, 2004; HORBELT *et al*., 2019; HORBELT *et al*., 2022), the excreted seeds stick to branches and, over the next several months, form a holdfast that provides stability as the mistletoe penetrates the host (THODAY, 1951; HEIDE-JØRGENSEN, 2008; TEIXEIRA-COSTA, 2021). During the first two years of development, the mistletoe grows primarily endophytically, with the exophyte later beginning to fork during the fourth year (NIERHAUS-WUNDERWALD &

LAWRENZ, 1997). The haustorium consists of parenchymatous cells in which bands of tracheids are embedded for the uptake and transfer of water and dissolved salts (SMITH & GLEDHILL, 1983; TEIXEIRA-COSTA, 2021; **Figure 3**).

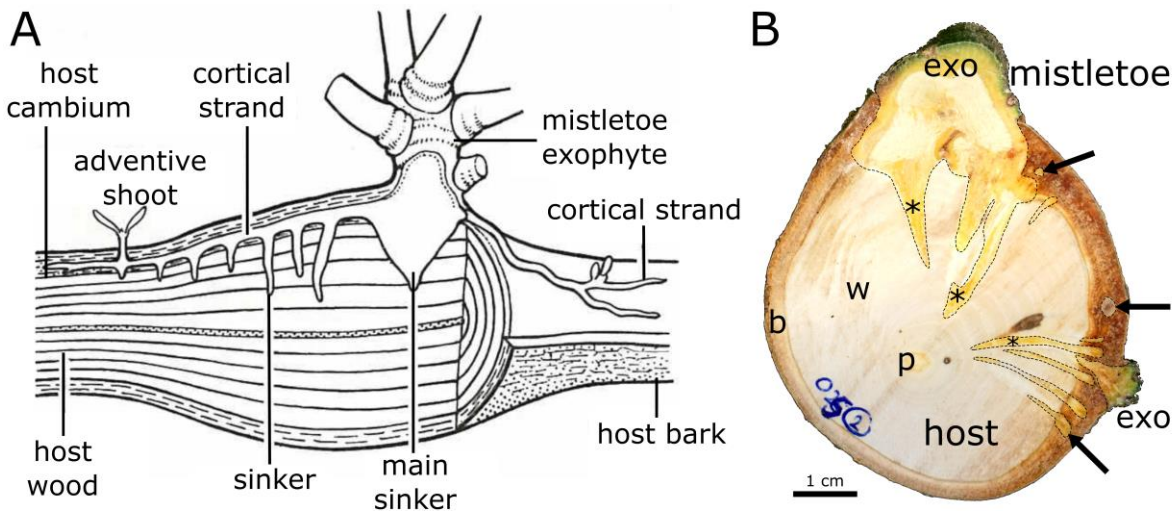

Figure 3: Schematic representation of the endophyte and exophyte of a European mistletoe (*Viscum album*) and its host (**A**; adapted from NIERHAUS-WUNDERWALD & LAWRENZ, 1997) and a photographed transverse section through a host branch (*Aesculus flava*) parasitized by *V. album* (**B**). The pith (p), wood (w), and bark (b) of the host are marked. In the mistletoe (tissues outlined in dashed lines), the upper exophyte (exo) grown from a seed transistions into the haustorium, which is divided into sinkers (examples are marked by asterisks) and cortical strands (examples are marked by arrows) that run through the host bark. The adventive shoot of the mistletoe on the right has emerged from a cortical strand.

Plants of the European mistletoe can reach an age of up to 30 years, growing into visible green leafy spheres of more than two meter in diameter (HEIDE-JØRGENSEN, 2008). During this process, not only the exophyte grows, but also the endophyte and the connected host branch, which becomes visible by a marked hypertrophy around the connection site (**Figure 3A**; NIERHAUS-WUNDERWALD & LAWRENZ, 1997). Dozens of new mistletoes can grow on a single host tree per year, resulting in host trees parasitized by several hundred mistletoes (VALLAURI *et al.*, 2002). In addition to mistletoes growing from germinating seeds, adventive shoots are present that grow from cortical strands. These extend from the penetration site of the mistletoe acropetally and basipetally through the cortex and bark of the host branch. For the host tree, severe mistletoe parasitization is not only accompanied by the depletion of water and nutrient salts, but also results in additional mechanical stresses from the mistletoe's weight and the wind loads caused by the large number of mistletoe leaves, even in seasons when the tree has shed all its own leaves.

Despite these mechanical stresses and the competition between the mistletoe and its host for the available space at and around the attachment site, failure of the mistletoe-host connection has to my best knowledge not yet been described in literature, nor has it been observed during my fieldwork. When failure occurs, the host branch always breaks off together with the mistletoe, indicating that the mistletoe-host connection is highly mechanically optimized and continuously able to adapt to the joint development and competitive growth over its entire lifetime. This makes the mistletoe-host interface an ideal model for damage prevention analyses in plants.

Numerous publications can be found on the anatomy and morphology of mistletoes (see, amongst others, the literature cited above) and on the ecological and economic importance of parasitic infestations of crops (SCHOLES & PRESS, 2008; BELL & ADAMS, 2011; PARKER, 2012; CLARKE *et al*., 2019; WATSON *et al*., 2020). However, findings concerning their mechanics are scarce. Infestations of the dwarf mistletoe (*Arceuthobium americanum*) have been described as having effects on the mechanical properties of host wood (PIIRTO *et al*., 1974). Studies characterizing the mechanics of mistletoe-host connections (or other parasitic plants) have to my knowledge not yet been published.

2.1.3 Damage management

During its evolution, nature has developed various mechanisms to deal with the occurrence of damage. One ability that can be found in a wide range of plants is the structural and functional self-repair of wounds. Furthermore, some species shed dysfunctional or no longer needed organs (‘abscission’).

2.1.3.1 Self-repair

The repair processes that take place after a mechanical injury can be divided into an initial fast sealing of the wound, followed by a subsequent slower healing phase. The purpose of the sealing phase is to minimize water loss and to protect the wound from infection by pathogens (SPECK & SPECK, 2019). Physical responses that can act within seconds and minutes can cause the deformation of entire organs (SPECK *et al*., 2018; HESSE *et al*., 2020) or of their wounded parts (ANANDAN *et al*., 2018), can push cells into the damage-induced fissures (BUSCH *et al*., 2010), and/or can result in the release of plant saps (such as latex or mucilage) that cover the wound (ANANDAN *et al*., 2018). The purpose of the healing phase is structurally to repair the damage and to ensure the mechanical integrity of the injured structure through

more complex and time-consuming chemical activities (e.g., latex coagulation; BAUER & SPECK, 2012; or local lignin synthesis around the wound; PAUL-VICTOR *et al.*, 2017) and growth processes (formation of a boundary layer or wound periderm; COUTANT, 1918; ANANDAN *et al.*, 2018; SPECK *et al.*, 2020).

Different equations are used to quantify the mechanical healing efficiency of the respective variables, incorporating either their values in unwounded and healed states (LUCAS *et al.*, 2016; SPECK *et al.*, 2020) or, additionally, directly after (artificial) wounding (DIESENDRUCK *et al.*, 2015; COHADES *et al.*, 2018).

2.1.3.2 Abscission

Abscission is a three-part process of the shedding of plant organs that might be damaged or no longer functional. It includes (i) the resorption of some of the nutrients still present in the organ, (ii) the detachment of the organ within a distinct abscission zone and sometimes with the assistance of enzymatic cell wall degradation (SEXTON & ROBERTS, 1982), and (iii) the suberin and/or lignin reinforcement of cells to form a protective layer around the abscission site (**Figure 4**; ADDICOTT, 1982; SHTEIN *et al.*, 2019). This protection can develop before and/or after the shedding of the organ.

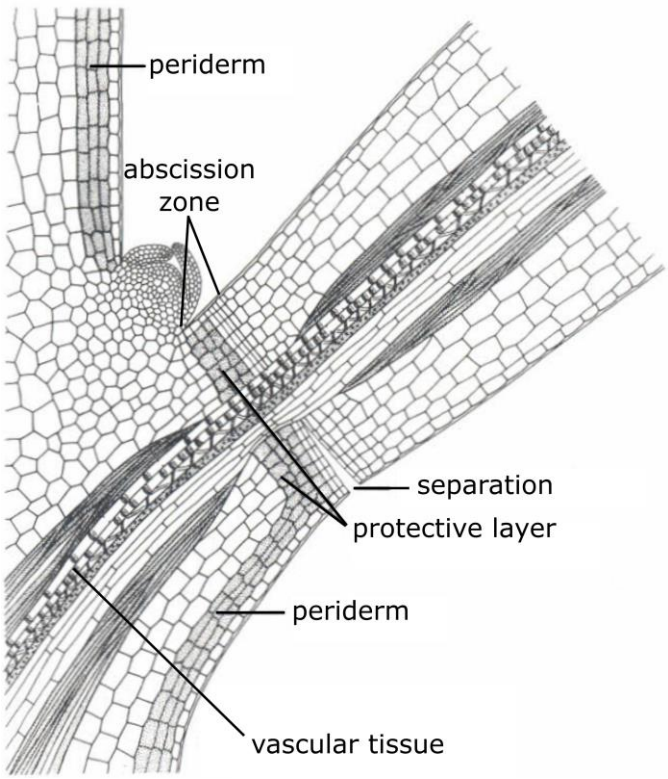

Figure 4: Drawing of a typical leaf abscission site. The protective layer that seals the resulting wound emerges from the adjacent periderm layers. Adapted from ADDICOTT, 1982.

2.1.4 Opuntioideae

The cactus family (Cactaceae) is united by their succulent growth forms and anatomical, physiological, and reproductive adaptations to survive with little or only seasonally available water (REBMAN & PINKAVA, 2001; NOBEL, 2002). It includes more than 1700 species (CHRISTENHUSZ & BYNG, 2016), with the Opuntioideae forming the second largest subfamily (after the Cacteae). The distinctive feature of the Opuntioideae is their growth habit with chained branches and distinct constrictions at the junctions. Anatomically, they are characterized by xerophytic adaptations, such as a multilayered hypodermis, a branch geometry that allows rapid water storage, and the abundant presence of oxalate crystals and mucilage glands (BENSON, 1982; GIBSON & NOBEL, 1986; NOBEL, 2002).

The shape of their branches was the naming characteristic for two of the most important subfamilies: The Cylindropuntieae with their almost cylindrical branches and the Opuntieae (also referred to as Platyopuntias) with flat branches that have an approximately oval cross-section (MAUSETH, 2006). During evolution, various reproductive strategies have evolved within the Opuntioideae. In many species, such as in *Opuntia ficus-indica* (**Figure 5A**; BOBICH & NOBEL, 2001a), also known as the 'prickly pear' with fruits that have become increasingly popular as edibles in Europe, reproduction is mainly sexual through flowers, fruits, and seeds (BARBA *et al*., 2020). However, some species, especially but not exclusively within the Cylindropuntieae, reproduce mainly asexually (BOBICH & NOBEL, 2001b; REBMAN & PINKAVA, 2001). In these species, new offshoots grow by vegetative propagation from fallen branches. A high rooting and establishment rate of shed branches is also found for some species that are known for their primarily sexual reproduction, indicating that mixed reproduction modes exist (EVANS *et al*., 2004). In species with particularly pronounced vegetative reproduction, such as *Cylindropuntia bigelovii*, also known as the 'jumping cholla' because their branches abscise under slight mechanical impacts and give passing ramblers the impression that they actively jump, several hundreds of small offshoots can be found in the vicinity of larger plants (**Figure 5B**; BOBICH & NOBEL, 2001b). Some vegetatively propagating species have so-called propagules with barbed spines that can become entangled in the fur of passing mammals and be carried away before falling off and growing into a new plant, enabling propagation over lager distances (GIBSON & NOBEL, 1986; CROFTS & ANDERSON, 2018).

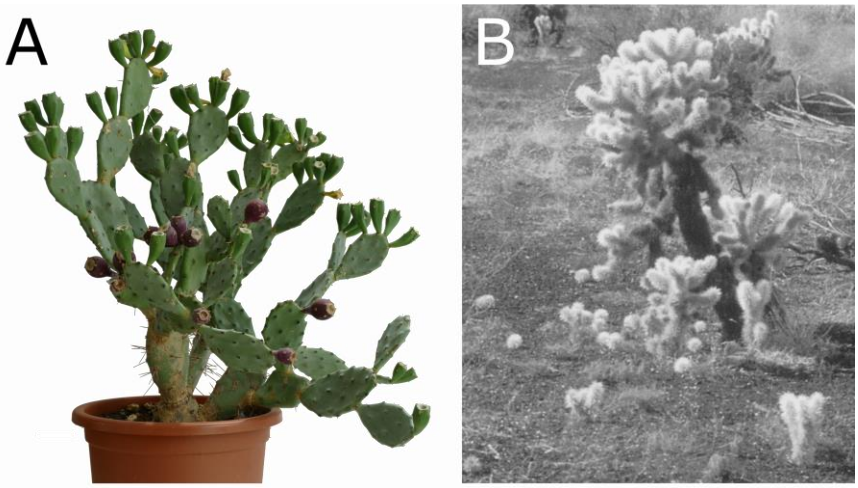

Figure 5: Experimental plant of *Opuntia ficus-indica* including purple fruits (**A**; adapted from **Manuscript A**) and a wild plant of *Cylindropuntia bigelovii* with several detached branches rooted as clonal offshoots in its close vicinity (**B**; adapted from REBMAN & PINKAVA, 2001).

The various propagation modes of the Opuntioideae are accompanied by the general advantages and disadvantages of sexual and asexual reproduction. Sexual reproduction leads to greater variability in the resulting seedlings via recombination of genetic material, allowing the species to adapt to changing environmental conditions. Asexual reproduction produces clones that do not involve recombination of genetic material but require less energy (YANG & KIM, 2016). Additionally, the propagation modes are closely related to the mechanical behavior of their branch-branch junctions, because lateral branches can serve as offshoots or are required to bear flowers and fruits (**Figure 5**).

2.1.4.1 Branch-branch junctions of Opuntioideae

Mechanical analyses of branch-stem junctions of columnar cacti and supporting finite element analysis of their ramification models have shown that these transition zones are not a region of mechanical weakness (SCHWAGER *et al*., 2013). In contrast, NOBEL & MEYER (1991) have performed bending tests with fixed and non-fixed branch-branch junctions of *O. ficus-indica* and revealed that these are, indeed, distinct mechanical weak points. However, comparative field analyses have shown that marked mechanical differences, even between closely related species, of these junctions are present within the Opuntieae. Much higher forces were required, for example, to deflect and break off lateral branches of *O. ficus-indica* (40 to 100 N for failure) compared with those of *O. occidentalis*, a hybrid daughter species that reproduces mainly vegetatively (5 to 15 N for failure; BOBICH & NOBEL, 2001a). Comparable bending tests have been carried out on various species of Cylindropuntieae,

revealing that those species in which vegetative propagation plays a greater role tend to have less rigid junctions that fail under lower forces (2 to 8 N in *C. bigelovii*; BOBICH & NOBEL, 2001b). In these bending tests, the forces required for the deflection and failure of the respective junctions were quantified; however, calculations of the geometry-independent mechanical variables (such as strength or elastic modulus) were not possible because of the complex geometry and the rather low length-to-diameter ratios of the samples (which should at least be at about 20 for valid calculations; NIKLAS, 1992).

2.1.4.2 Self-repair in Opuntioideae

The aerial organs of most Opuntioideae are protected from infestation by herbivores and from water loss by a waxy cuticle, an epidermis, and a multilayered hypodermis with thick cell walls (NOBEL, 2002). If these tissues are injured, cacti, like most other plants, do not heal by direct replacement. Instead, the wound meristem grows peridermal wound tissues to repair them, providing protection initially by the formation of water-impermeable suberin and, in later stages, by the lignification of the cell walls (BLOCH, 1941; GINZBERG, 2008). More than a century ago, COUTANT (1918) schematically outlined the anatomical healing processes for artificially injured branches of *Opuntia versicolor* and *O. discata*, showing the way in which the wound tissue sealed the fissure and adopted a protective function of the epidermis and hypodermis (**Figure 6**).

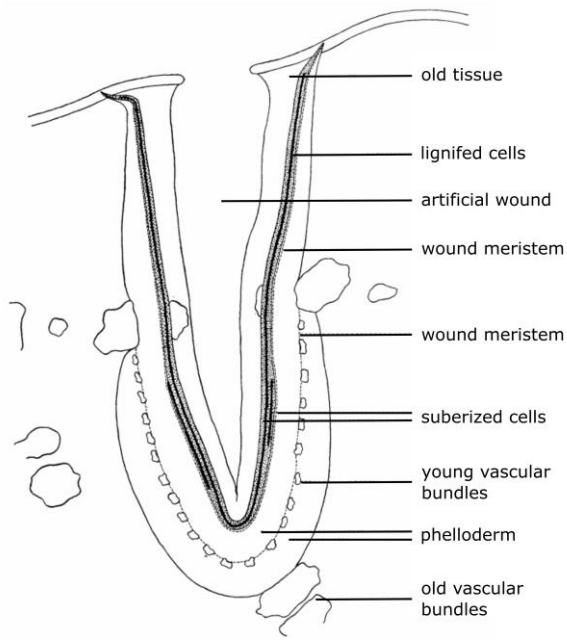

Figure 6: Drawing of a transverse section through an artificially wounded *Opuntia versicolor* branch after 31 days of healing. Dead cells remain inside the wound, while a suberized and lignified protective layer has developed from the underlying wound meristem. Adapted from COUTANT, 1918.

In addition to the lack of detailed analyses at a cellular level, there are, to the best of my knowledge, no studies on the restoration of the mechanical integrity of injured branches of Opuntioideae after injuries.

2.1.5 Damage control in plants as a source of inspiration

The Cambridge dictionary defines 'longevity' not only as 'living for a long time', but also as 'remaining […] useful for a long time' (CAMBRIDGE UNIVERSITY PRESS, 2022). During the more than 400 million years of the evolution of land plants (MORRIS *et al*., 2018), various mechanisms of damage control have evolved to maintain the plants' functionality for as long as possible ('damage prevention') or to recover it after damage ('damage management'), thus ensuring their survival and competitiveness. The concepts behind some of these mechanisms have been used as biomimetic inspiration to increase the longevity of technical applications. Damage prevention by bio-inspired gradient structures has been used, for example, by HORN *et al*. (2019) to modify the internal structure of concrete at various hierarchical levels (porosity, arrangement of reinforcing fibers), resulting in material and energy savings of up to 40%. Damage management concepts from nature have also made their way into technical applications: The self-repair mechanism of the Dutchman's pipe vine (*Aristolochia macrophylla*), in which parenchymatous cells squeeze into lesioned tissue in order to seal it (BUSCH *et al*., 2010), served as the model for a bioinspired self-sealing polyurethane foam with a repair efficiency of 99.8% at 1 bar overpressure (RAMPF *et al*., 2013).

Bioinspired material systems are not *per se* sustainable but have great potential for material and energy efficiency (SPECK *et al*., 2017). They can thus contribute to sustainably designed material for use in our current human-dominated epoch of the 'Anthropocene' and, thereby, to the achievement of the climate targets of the 2030 Agenda and its Sustainable Development Goal ('SDG'; UNITED NATIONS, 2016) (**Article B**). The aim of this thesis has been to analyze the two presented plant systems, namely the mistletoe-host connection and the cacti branches with their junctions, in order to create profound knowledge of their underlying damage control mechanisms. This knowledge can be abstracted in follow-up projects, translated into an engineering language, and transferred into technical materials systems with enhanced longevity properties.

3 MATERIAL AND METHODS

The following section lists the materials and methods used in the articles and the manuscript presented in **Part II**. To avoid duplicate listings and to facilitate a comparison of the methods, the order is based on the mode of analysis and is then differentiated between experimental plants.

3.1 Plant material

3.1.1 Mistletoe-host samples

All 130 mistletoe samples were all harvested from a single host tree (*Aesculus flava* SOL.) in the Botanic Garden of the University of Freiburg (Germany) between May and August 2020. The age of the mistletoe was estimated based on the number of branchings (one branching per year is formed from the age of four; **Figure 7A**). The sex of the dioecious mistletoe was determined by the type of flower and the presence of berries on the plant. This distinction was not yet apparent in some plants that were six years old or younger, and so they were classified as 'juvenile'.

3.1.2 Cacti samples

All experimental cactus plants of *Opuntia ficus-indica* (L.) MILL. and *Cylindropuntia bigelovii* (ENGELM.) F.M. KNUTH were purchased from Kakteenland Steinfeld (Germany) and assigned with an accession number (*O. ficus-indica*: 5400-01; *C. bigelovii*: 5400-02). Plants were cultivated under controlled conditions in a phytochamber (12/12 h dark/night cycle; day conditions: 30% RH and 30 °C; night condition: 50% RH and 20 °C) at the Botanic Garden of the University of Freiburg for at least six months prior to sampling. The exception was one large plant of *C. bigelovii* that was used for junction tensile tests and that grew in a greenhouse of the Botanic Garden (natural day-night rhythm; RH: 52.3 ± 13.1%; temperature: 18.8 ± 8.5 °C; both mean values ± standard deviation). All plants were in a well-watered condition at the times of the experiments. Because of frequent hybridization, polyploidy, and associated taxonomic difficulties in the genus *Opuntia* (MAJURE *et al*., 2012; GUERRERO *et al*., 2019), our experimental *Opuntia* plants were genetically sequenced and confirmed as species *O. ficus-indica* (sequencing details can be found in **Article D**).

3.1.2.1 Artificial wounding of cacti branches

For the anatomical and morphological self-repair analyses of the lateral cactus branches, artificial circumferential wounding was applied with a scalpel. The position of the wound was at 50% of the branch length for all anatomical analysis and the mechanical tests on *O. ficus-indica* and at 25% (measured from the junction) for the mechanical analysis of *C. bigelovii*. Based on preliminary experiments quantifying the tissue proportions of branch cross-sections, a relative depth of cut of 10% of branch diameter was chosen for *C. bigelovii* and 15-20% for *O. ficus-indica*. These cuts were intended to injure the dermal tissue (epidermis and hypodermis) and most of the cortex parenchyma but to leave the vascular bundles and pith intact.

3.2 Morphometric analyses

3.2.1 Mistletoe-host connection

For the morphometric analysis of the mistletoe-host attachment site and the quantification of hypertrophy in this region, the diameter of the host branch was measured acropetally (d_{acro}) and basipetally (d_{basi}) to the hypertrophic region and directly at the mistletoe attachment (d_{max}; twice each with orthogonal offsets). The lengths of the hypertrophic region (l_{hyp}) and the thickness of the basal mistletoe branch were also measured (d_{mist}) (**Figure 7B**). All measurements were conducted using a digital caliper (Mitutoyo Absolute Digimatic, measuring accuracy: ±0.03 mm, Kawasaki, Japan).

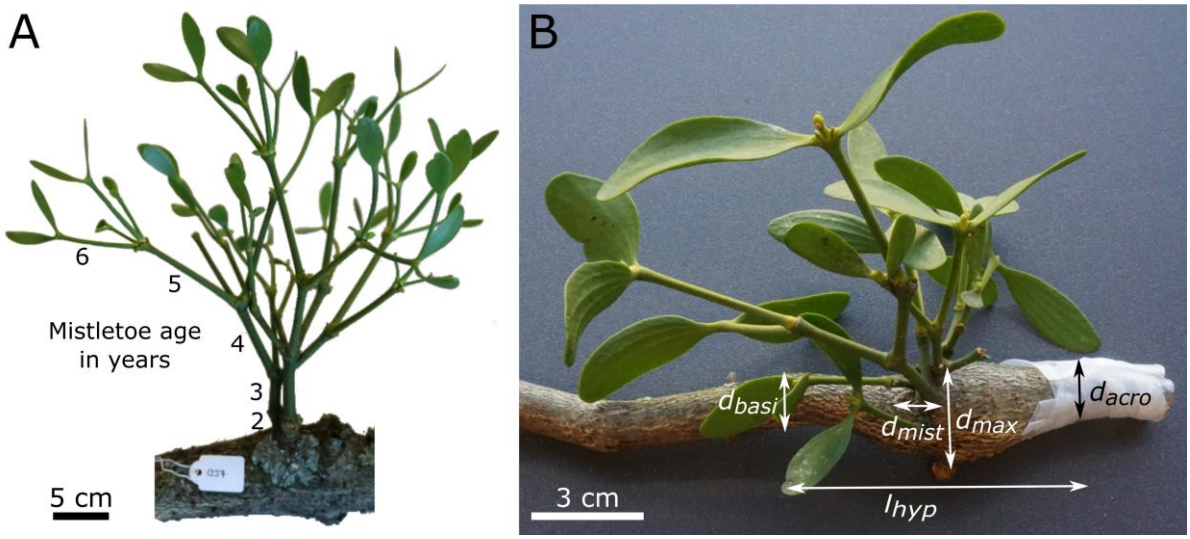

Figure 7: Examples of determinations of misteltoe age in years via the number of branchings (**A**) and the measured morphological variables of mistletoe and hypertrophic region of the host branch (**B**). Adapted from **Article C**.

3.2.2 Branch-branch junctions of cacti

Twelve lateral branches each, without leaves and periderm formation at the branch surface, and the attached junctions of *O. ficus-indica* and *C. bigelovii* were morphometrically analyzed. Based on images, the cross-sectional area of the junction and the branches at their widest point [mm²], the ratio between these values [/], the length of the major axis *a* [mm] (longest axis passing through the centroid) and minor axis *b* [mm] (normal to the major axis through the centroid), and the axial second moment of area with regard to these axes ($I_{major\text{-}axis}$ and $I_{minor\text{-}axis}$ [mm^4]) were measured using the software Fiji (ImageJ version 1.53c; SCHINDELIN *et al*., 2012). From these data, the respective torsional constant *K* [mm^4] was calculated for an elliptically approximated cross section (for the junctions of both species and the branches of *O. ficus-indica*):

$$K_{ellipse}\ [mm^4] = \frac{\pi * a^3 * b^3}{a^2 + b^2}$$

or a round approximated cross section (for the branches of *C. bigelovii*):

$$K_{circle}\ [mm^4] = \frac{\pi * r^4}{2}$$

with *r* [mm] calculated as the radius of the measured cross-sectional area.

3.3 3D imaging techniques

Three different techniques were used for 3D imaging of the plant samples, with one technique capable of imaging the surface of the samples (3D scanner) and two techniques also imaging the location of internal tissues (µCT and MRI).

3.3.1 Mistletoe-host connection

3.3.1.1 X-ray microtomography (µCT)

Three-dimensional visualizations of the mistletoe tissues inside the host branch were acquired at three different ages of the mistletoe (4, 8, and 17 years) by using X-ray microtomography (µCT). The youngest sample was scanned with a Bruker scanner (SKYSCAN 1272, Bruker Corporation, Billerica, MA, United States) and a resolution of 10 µm. Because of the larger test chamber required, the two older samples were scanned with a Nikon scanner (XT H 160, Nikon, Chiyoda, Japan) and a resolution of 86 µm. Detailed scan and reconstruction settings can be found in **Article C**.

The high spatial resolution of the scan of the young mistletoe allowed tissue segmentation based on the reconstructed µCT gray-scale images. However, reference images of the cross sections were required because of the small density differences (and associated brightness values of the µCT images) between the mistletoe tissues and the bark of the host branch. For this purpose, after being scanned, the sample was sawed into cross sections (with respect to the host branch), and an image was taken every 1 mm with a stereomicroscope (SZX9, Olympus K. K., Shinjuku, Tokyo, Japan). Mistletoe tissue appeared greenish on these images and could be easily distinguished from brownish host wood and bark, allowing these images to be used as a reference for parts that were difficult to segment. Segmentation of mistletoe and host tissues was performed using Avizo software (version 2020.2, Thermo Fisher Scientific, Waltham, MA, United States).

3.3.2 Cacti branches

3.3.2.1 3D scanner

The external geometry of the lateral and sub-lateral cacti branches and their connecting junction was captured using a portable 3D scanner (Artec Spider). The accompanying software (Artec Studio 12 Professional, version 12.1.6.16, both Algona GmbH, Stuttgart, Germany) was used to merge multiple individual scans for better resolution, to fill possible holes, to compress the resulting finite element (FE) models to a maximum of 10,000 nodes, and to save them as STL files. Based on the resulting models, 3D-printed clamp attachments with perfect form fit were fabricated for bending and tensile tests (see **chapter 3.5.2.1**).

3.3.2.2 Magnetic resonance imaging (MRI)

Preliminary experiments showed that µCT scans of the cactus junctions did not provide meaningful images because of the high content of oxalate crystals (outshining all other tissues; PIERANTONI *et al*., 2019) and the very low density differences (and thus gray-value differences in µCT images) between the vascular bundles and parenchyma in *C. bigelovii*.
Magnetic resonance imaging (MRI) was therefore used for 3D tissue visualization of the cactus branches and their junctions. One overview scan and one surface coil scan (smaller measurement volume with higher spatial resolution) of the lateral branches and their junctions were conducted for each of the two cactus species. Scans with a small animal scanner (Biospec 94/2, Bruker, Billerica, MA, USA) resulted in a resolution between 67 and

160 µm and were acquired with a FLASH sequence. A detailed listing of the scan settings can be found in **Article D**. Based on the MRI gray-scale data, semiautomated segmentation of dermal tissues (consisting of epidermis and hypodermis), vascular bundles, and, if present, periderm tissue was performed for each scan using Avizo software.

3.4 Anatomical analysis

Techniques for 3D imaging (µCT and MRI) of plant structures provide a spatial overview of the location of the tissues involved. However, their resolution is not sufficient for (sub-)cellular imaging or for the detection of specific biopolymers (such as lignin). Light microscopic analysis of stained sections (fresh or embedded samples) provided these insights.

3.4.1 Mistletoe-host connection

For anatomical analysis, small blocks with edge lengths of about 10-15 mm, consisting of the mistletoe haustorium and its host wood, were sawed to size. These were embedded in polyethylene glycol and sections of about 10 µm thickness were cut using a rotary microtome (HistoCore BIOCUT, Leica Biosystems GmbH, Nussloch, Germany) and stained with toluidine blue (stains lignified cells blue-green and non-lignified cells red-purple) or acridine orange (stains lignified cells light yellow/orange and non-lignified cells brown/red). As a lignin detection method, additional sections were prepared by hand and stained with phloroglucinol and hydrochloric acid (stains lignified cells red; all other cells remain unstained). The sections were analyzed and captured by using various light microscopes. Detailed staining procedures and instrument specifications can be found in **Article C**.

3.4.2 Cacti branches

For the anatomical analyses of the self-repair experiments on the cactus branches, tangential cross-sections with a thickness of about 75 µm of unwounded, freshly wounded, and repaired (after 10 repair intervals ranging between 5 hours to 31 days) samples were cut using a cryostat (MEV, SLEE medical GmbH, Mainz, Germany). After the samples had been bleached with a 50% bleach solution (Eau du Javel, Floreal Haagen GmbH, Wadgassen, Germany), they were stained with a combination of safranin O and astra blue (staining woody cell walls red and cellulose walls blue) or for lignin detection with phloroglucinol and hydrochloric acid and then analyzed and captured using various light microscopes.

The same protocol, but without the phloroglucinol stains, was used to obtain microscopic sections of the junctions of *O. ficus-indica*. In addition to longitudinal sections, transverse serial cuttings were prepared through junction samples. For the anatomical analysis of *C. bigelovii* junctions, none of the standard methods could be used because of the very high mucilage content of the samples and the large mechanical difference between the hypodermis and adjacent parenchyma. Instead, the samples were embedded in hydroxyethyl methacrylate and polyethylene glycol distearate. Tangential sections of 3 µm thickness were prepared using a rotary microtome (RM 2065, Leica, Wetzlar, Germany).

A detailed description of the embedding, cutting, and staining techniques, together with the microscopes and imaging software used, can be found in **Article A** for the self-repair analyses and in **Article D** for the junction analyses.

3.5 Biomechanical testing

3.5.1 Mistletoe-host connection

Of all the collected mistletoe-host samples, 70 samples with the most suitable growth form were selected for mechanical analysis. 39 were tested as 'intact samples' (**Figure 8A**). Because the other 31 samples were too large for the clamping device, a slice (transverse section of the host branch) of 5-8 mm thickness was cut out of the center of the mistletoe-host attachment ('sliced samples') (**Figure 8B**).

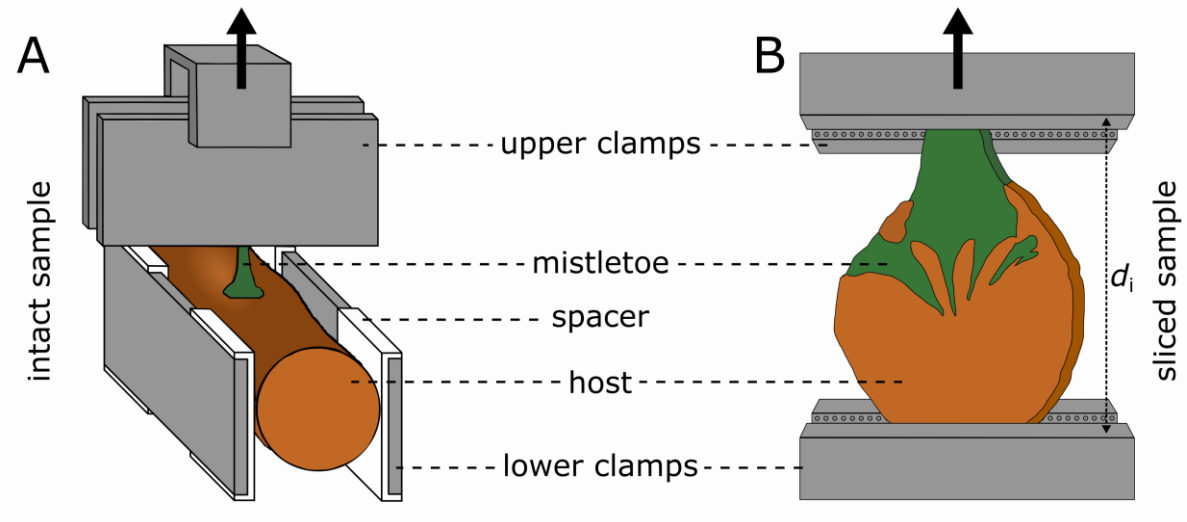

Figure 8: Schematic representation of the tensile tests on the mistletoe-host connection. The misteltoe (green) was fixed in the upper clamps and the host branch (brown) was fixed in the lower clamps. The tests were performed on intact samples (**A**) and cut sliced samples through the attachment zone (**B**). The additional spacers in (**A**) minimized the stresses caused by clamping around the misteltoe-host interface. Adapted from **Article E**.

3.5.1.1 Tensile tests

Regardless of their preparation, all samples were clamped in the universal testing machine (Inspekt Retrofit, Hegewald & Peschke, Nossen, Germany; equipped with a 10 kN load cell) in such a way that only mistletoe tissue was fixed in the upper clamps, and only host tissue was fixed in the lower clamps. The tensile direction was aligned as orthogonally as possible on the mistletoe outgrow of the host. For the intact samples, the host branch was sawed to a length between 6 and 14 cm, and the basal mistletoe branch was trimmed to a length between 2 and 5 cm. 3D-printed spacers (RGD450 as printing material; printed with Objet260 Connex3, Stratasys, Eden Prairie, MI, USA) were attached between the outer ends of the host branch and the clamps to minimize stresses attributable to clamping at the mistletoe-host interface (**Figure 8A**). The tensile speed was set to 1 mm/s, and the test ended after complete failure of the sample. Force and displacement values were recorded at 50 Hz.

Additionally, fourteen plain wood samples (nine tested parallel to host grain, and five tested normal to wood grain) from uninfected branches of the host tree *A. flava* were sawed to a dog-bone shape and were subjected to tensile testing for failure.

3.5.1.2 Fracture surface quantification

After failure of the samples, one of the two resulting fracture surfaces was scanned by digital microscopy (Smartzoom 5 and corresponding Zen2.6 pro software, both Carl Zeiss AG, Oberkochen, Germany) at a resolution between 0.007 and 0.002 mm. The resulting 3D model was imported into Meshlab software (version v2020.07; CIGNONI *et al.*, 2008) in order to trim the surface free from surrounding noise and to quantify the surface area (**Figure 9**). In addition to this rough surface (A_r [mm²]), the corresponding flat surface (A_c [mm²]) was measured by removing the height dimension of the data (resulting in a flat projection of the 3D surface). The roughness R [/] of the fracture surface was calculated as:

$$R = \frac{A_r}{A_c}$$

Between mechanical testing and fracture surface analysis, samples were either stored moist and cool for a maximum of five days or remoistened by brief immersion in water prior to scanning. Comparative preliminary tests showed that the median error for rewetting was 0.3% (interquartile range: 6.6%), and so the data from both groups were pooled.

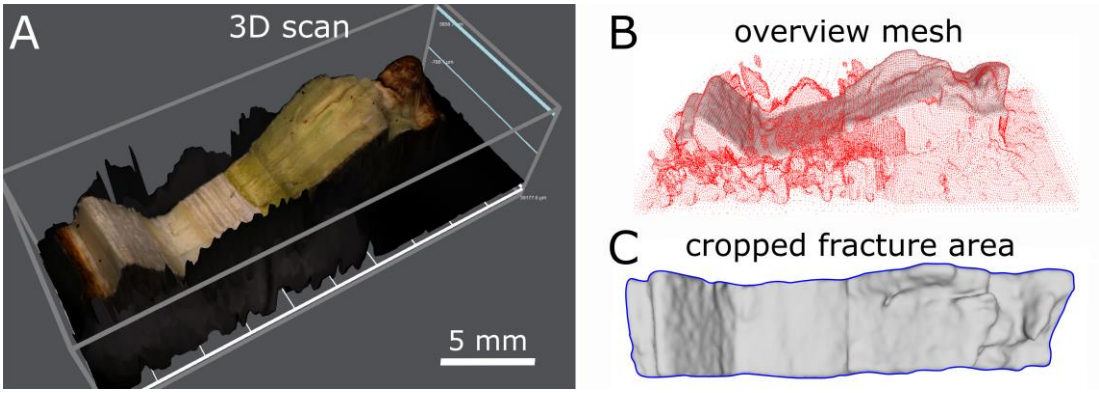

Figure 9: Fracture surface measurement of a sliced sample by using digital microscopy. The generated 3D scan (**A**) was converted into a mesh file (**B**). The cropped surface (**C**) was measured after removal of the ambient noise (red dots outside gray area). This enabled a roughness calculation of the fracture surface. Adapted from **Article E.**

3.5.1.3 Mechanical variables

Based on the force-displacement curves, the maximum force F_{max} [N] and axial rigidity k [N] (which, in comparison with the axial stiffness, is not normalized to the initial length d_i of the sample) were calculated using the following formula:

$$k = \mathrm{E} * \frac{A}{d_i}$$

with Young's modulus E, cross-sectional area A, and $E * A$ determined as the slope of the linear elastic range of the force-displacement curve (before the main peak). Tensile strength σ_{max} was calculated using the following equation:

$$\sigma_{max} = \frac{F_{max}}{A}$$

The work of fracture W [Nm] was calculated via the integral under the force-displacement curve. The fracture energy E_f [J/m²] was calculated by normalizing over the fracture area:

$$E_f = \frac{W}{A}$$

Tensile strength and fracture energy were normalized over both the rough (A_r) fracture area and the corresponding (A_c) fracture area. The sample strain values were calculated over the initial sample length d_i and were used to determine the sample strain at failure ε_f [%] values (as strain at maximum stress).

Detailed information on the tensile tests, the fracture area measurements, and the calculation of the mechanical properties of the mistletoe-host connections are presented in **Article E**.

3.5.2 Cacti branches

Repeated bending tests were performed on the branches of the two selected cactus species to quantify their self-repair efficiency. Tensile tests were used to characterize the most mechanically important tissues (dermal tissue and vascular bundles) and the branch-branch junctions.

3.5.2.1 3D-printed clamp attachments

Tensile tests on biological samples are often susceptible to slipping artifacts, as mechanical damage to individual tissues or the entire sample can occur if the samples are clamped too tightly. In addition, the geometry is not standardized according to DIN or ISO form standards. Likewise, during (two-point) bending tests, both the fixation of the samples and the application of the force in a reproducible manner can be challenging. For the repeated bending tests and for the tensile tests on the branch junctions of the cacti, we used individually customized, 3D-printed clamp attachments to minimize slipping events by providing the optimal form fit between sample and clamps (**Figure 10**).

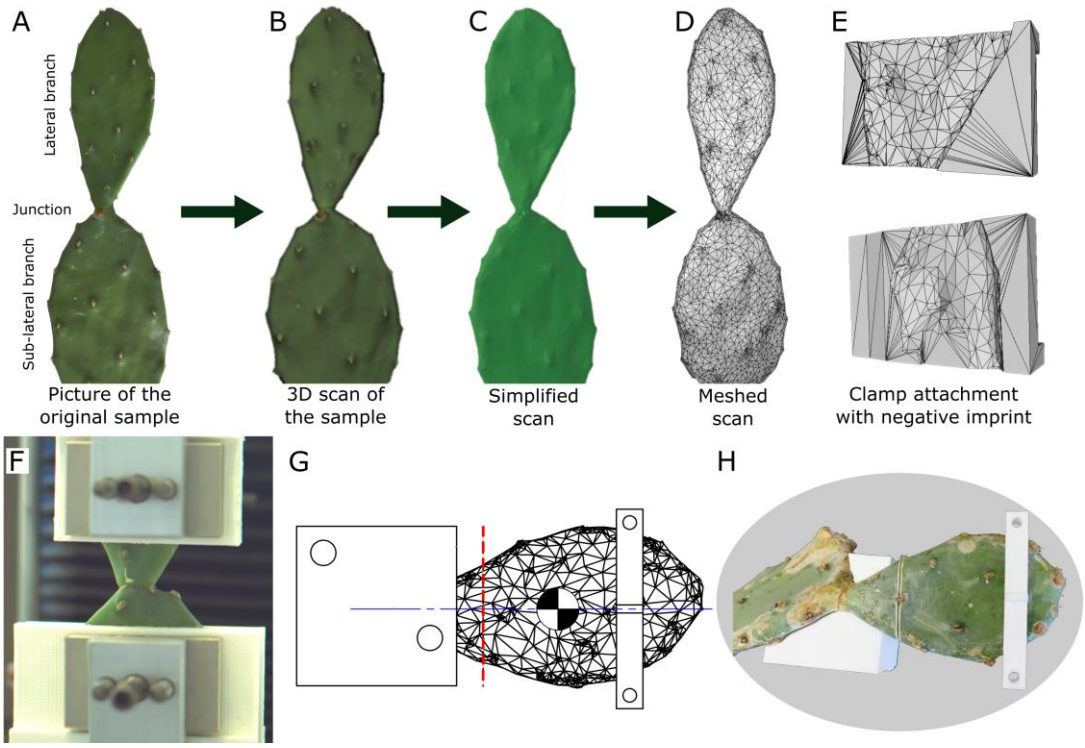

Figure 10: Printed clamp attachments based on 3D scanned cactus branch models. The lateral and sub-lateral branches (**A**) were 3D scanned (**B**), the mesh was simplified (**C**&**D**), and the clamp attachments were designed as negative imprints (**E**&**G**). The resulting attachments were printed and mounted between the branch and clamp during tensile (**F**) and bending (**H**) tests. The red dashed line in (**G**) indicates the location of the artificial wound, and the blue line is normal to the junction plant. Adapted from **Article A** and **Manuscript A.**

For this purpose, the lateral and sub-lateral branches on the experimental plant were initially 3D scanned (**Figure 10A**; **chapter 3.2.2.1**). Raw clamp models were constructed in CAD software, and the cactus models were imported (**Figure 10B**-**E**). The raw models were positioned on the geometry according to the test requirements (at defined distances from the artificial wound for bending tests and at defined distances from the branch junction for tensile tests; **Figure 10G**). The branch geometry was subtracted from the blanks, creating a cavity in the clamps. The resulting clamps with negative imprints were, for each sample, 3D-printed from a polylactic acid filament (Premium PLA, Formfutura BV, Nijmegen, Netherlands) by using an extrusion 3D printer (Pro2Plus, Raise 3D Technologies, Inc., Irvine, CA, USA) and attached between the clamp and the sample during the mechanical tests (**Figure 10F**&**H**).

3.5.2.2 Repeated bending tests

The ability of cactus branches to restore their mechanical properties by self-repair processes was investigated by means of repeated two-point bending tests on the same branches attached to the experimental plant. Fourteen lateral branches each of *O. ficus-indica* (divided between two plants) and *C. bigelovii* (divided between three plants) were tested in an unwounded state, a freshly wounded state (within 15 minutes after artificial wounding), and after a healing period of 21 days. The lateral branch-branch junction and parts of the lateral branch (up to 10 mm basal to the wound site) were fixed with 3D-printed clamps, and collars that had likewise been 3D-printed were attached 60 mm apical to the wound (**Figure 10 G**&**H**). Each collar was subsequently connected to a universal testing machine with a Kevlar thread. An interposed pulley enabled the vertical movement of the universal testing machine (Inspekt mini, Hegewald & Peschke Meß- und Prüftechnik GmbH, Nossen, Germany) to be converted into a horizontal bending force. During the experiments, experimental plants were positioned with the base-apex axis of the tested branches aligned parallel to the ground. For *O. ficus-indica* branches and their oval cross sections, forces were applied normal to the flat cladode surface.

Tensile speed was set to 1 mm/s with a total displacement of 10 mm. Force and displacement data were recorded at 50 Hz. From these data, the work W [N*mm] (as an integral under the force-displacement curve) required and the bending stiffness EI [N*mm²] of the branch were calculated. Since a biphasic behavior of the samples was found, the latter was calculated for

a first linear range (from 3.0 to 4.25 mm deflection) and a second linear range (from 6.5 to 9.5 mm deflection) according to the following formula:

$$EI = \frac{L^3}{3 * b}$$

with *L* being the length of the cantilever (60 mm for all samples) and *b* the slope of the respective linear interval in the force-displacement diagram.

To determine the effect of wounding on the mechanical properties of a sample, the wounding effect (*WE*) was calculated using the following equation:

$$WE[\%] = \frac{unwounded\ value - wounded\ value}{unwounded\ value} * 100\%$$

in which the respective values of work or bending stiffness in the unwounded (*uv*) and wounded state (*wv*) were inserted. For the wounded values, the values were inserted either immediately after wounding (wv_0) or after the 21-day repair phase (wv_{21}). The healing effect of the 21-day repair phase (HE_{21}) was calculated as the difference of the resulting wounding effects (WE_0 and WE_{21}):

$$HE_{21}\ [\%] = WE_0 - WE_{21} = \frac{HE_{21} - HE_0}{uv} * 100$$

3.5.2.3 Tissue tensile tests

The strength-determining cactus branch tissues, i.e., the dermal tissue (consisting of epidermis and multilayered hypodermis and, in older branches, a periderm coverage) and the vascular bundles, were mechanically characterized by isolating them from the branches and testing them under tensile loading to failure by using a microtensile testing machine. Twelve samples each of dermal tissue without periderm support and vascular bundles from the lateral branches of both cacti species were examined. For *O. ficus-indica*, additional tests were carried out to determine whether the orientation of the sample on the branch (longitudinal or transverse with regard to the main axis of the branch) had an influence on their mechanical properties (this was not possible for *C. bigelovii* because of the numerous tubercles on the branches), and the way in which peridermal coverage alters the mechanical properties of the dermal tissue (older branches with complete periderm coverage were not present on the experimental plants of *C. bigelovii* and therefore could not be tested). For the vascular bundles of *O. ficus-indica*, a distinction was made depending on whether these were taken from lateral branches ('young samples') or from basal branches that were completely

covered with periderm ('older samples'). All tissue samples were carefully removed using a scalpel.

Prior to tensile testing, the diameter or thickness of the samples (or a severed end section) was measured using stereo microscopic or light microscopic images, and their cross-sectional area (assuming a round cross-section for the vascular bundle samples and a rectangular cross-section for the dermal tissue samples) was calculated. The samples were glued to small metal plates, with a few seconds being allowed for the glue to dry (for the vascular bundle samples of *O. ficus-indica*, the glue took longer to dry, and the sample was kept moist during this time with the aid of a custom-built humidifier), and then mounted onto holders of a micro-tensile stage equipped with a 10 N or a 50 N load cell. The initial spacing of the plates was measured before the sample was tensile-loaded at 0.5 mm/s until failure, with the force and displacement being recorded at 100 Hz. The elastic modulus E [MPa], the tensile strength σ_{max} [MPa], the strain at failure ε_{max} [%], and the fracture energy G_f [mJ/mm²] were calculated from the recorded data and the respective cross-sectional areas. A detailed protocol for the diameter measurement, the processing of the force-displacement data, additional relative water content measurements, and the calculation of the mechanical variables can be found in **Article D**.

3.5.2.4 Junction tensile tests

The mechanical properties of the lateral branch-branch junctions of the cacti were analyzed using tensile tests to failure. For this purpose, 14 junctions with young lateral branches (with leaves still attached to the branch; divided between two plants) and 14 with older lateral branches (without leaves at the branches and with visible periderm formation at the junction; divided between two plants) of *O. ficus-indica* and 15 lateral junctions of *C. bigelovii* (all without leaves; coming from one plant) were taken from the experimental plants and tested within the next 20 minutes. The lateral and sub-lateral branches (**Figure 10A**) were cut to fit into the clamps of the universal testing machine (Inspekt mini, Hegewald & Peschke Meß- und Prüftechnik GmbH, Nossen, Germany; equipped with a 1 kN load cell for experiments on *O. ficus-indica* and a 100 N load cell for experiments on *C. bigelovii*), with an initial jaw spacing of 30 mm. The junctions were positioned centrally, with the tensile force acting normal to their cross-section. The spines were carefully removed before testing, and all cut surfaces were sealed using Parafilm® (Bemis, Neenah, WI, USA).

Tensile speed was set to 1 mm/s, and force and displacement data were recorded at 50 Hz. After sample failure, the lateral branches were weighed (Kern 440-45N, Kern & Sohn GmbH, Balingen-Frommern, Germany; reproducibility: 0.1 g), and the fracture surfaces were photographed and manually measured using Fiji software. In addition, the location of failure (through the junction, branch, or both) and the characteristics of the failure site (smooth, fibrous, or cup and cone) were differentiated. From the recorded data, tensile stiffness k [N/m], effective tensile modulus $\bar{E}$ [N/m² = Pa], maximum force F_{max} [N], tensile strength σ_{max} [N/m² = Pa], work of fracture W [Nm], fracture energy G_f [N/m], and strain at failure ε_f [%] were calculated for all three groups. Linear correlation analyses (Pearson's ρ) were used to examine the relationship between the mechanical variables and the mass of the lateral branch as an approximation of their age. A detailed protocol for the processing of the force-displacement data and the calculation of the mechanical variables can be found in **Manuscript A**.

3.5.3 Local strain analyses

Two-dimensional digital image correlation (2D DIC) was applied to measure local surface strains during the tensile loading of the sliced mistletoe-host samples and the cacti branch junctions. For this purpose, a stochastic speckle pattern was sprayed onto the surface of the samples to increase brightness contrast (**Figure 11**).

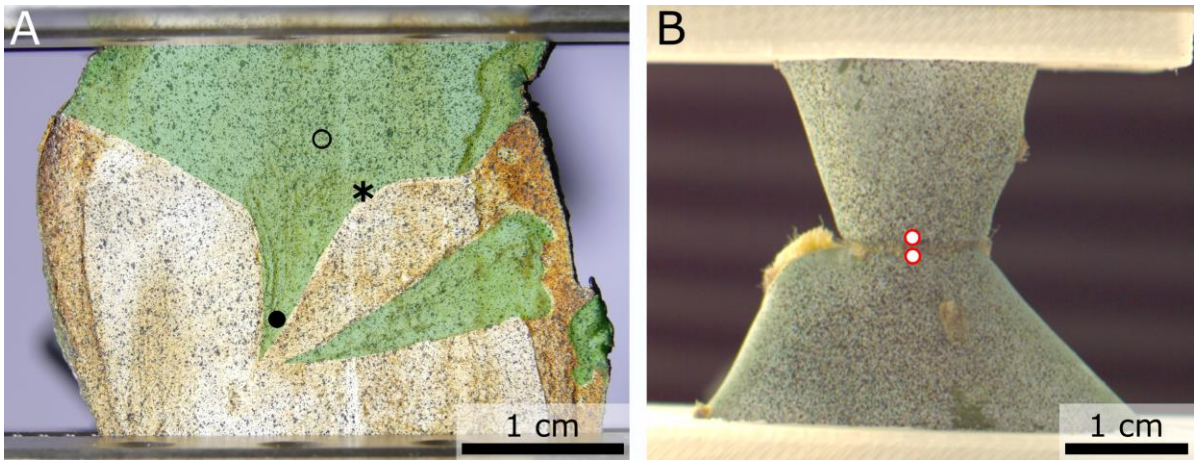

Figure 11: Sample preparation with a stochastic speckle pattern for digital image correlation analysis. (**A**) Sliced mistletoe-host sample with mistletoe tissue marked in green, and three points (open circle at sinker base; asterisk at mistletoe-host interface; filled circle at sinker tip) marked for detailed analysis. (**B**) Branch junction sample of *O. ficus-indica*. The points for detailed analysis of the cactus junction are shown as red dots with a white center. Adapted from **Article E** and **Manuscript A.**

During tensile testing, the samples were filmed frontally by a camera at 50 to 90 fps. The resulting image series was loaded into DIC software, and an image in the undeformed state was defined as the reference (**Figure 12A**). The DIC algorithms subdivided this image into small squares (so-called 'subsets'; indicated as red squares in **Figure 12**).

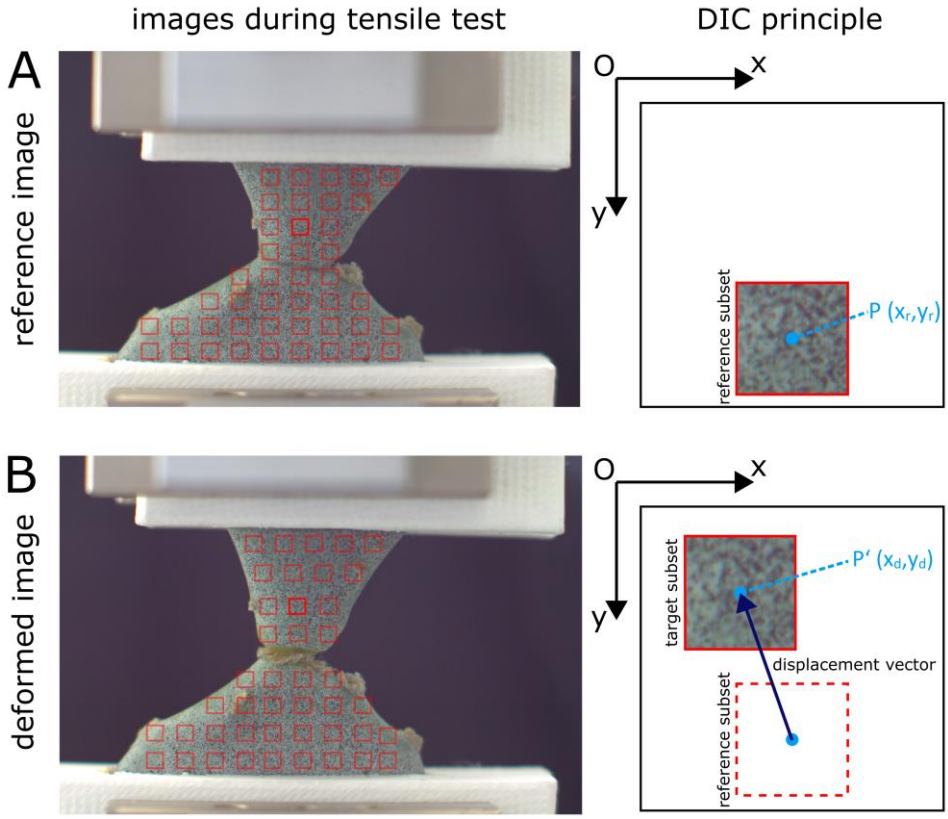

Figure 12: General principle of digital image correlation (DIC) algorithms. From the imported image stack, one image is defined as the reference image (**A**), and all other images are analyzed as deformation images (**B**). The surface of the sample to be analyzed (in the example shown with a sprayed random speckle pattern to increase contrast) is divided into small subsets (red squares). The position of the subsets in the deformed images is determined by correlation analysis of the gray-value patterns of the reference image. The resulting displacement vectors (an example of one subset is shown in the right panel of **Figure 12**; light red square in the left images) of the various subsets and their ratio to each other can be used to calculate the displacement and strain pattern of the respective image. Adapted from PAN *et al.*, 2009.

Correlation analysis of the gray-value patterns of these subsets allows the latter to be tracked across the stack of deformed images (**Figure 12B**). Local strains can be derived from the relative displacement between neighboring subsets. In addition to the strain measurements of the entire surface, detailed analyses can be performed of individual selected points (**Figure 11**) or sections through the surface. Detailed specifications of the cameras and the selected DIC settings can be found in **Article E** for the mistletoe-host connection and in **Manuscript A** for the cactus junctions.

3.6 Statistics

For the mistletoe analyses, statistical tests were used to perform correlation analyses of the various morphometric (**Article C**) and biomechanical (**Article E**) variables with sex and age of the mistletoes. In addition, statistical analyses were used to test for significant differences between the analyzed mistletoe groups (intact and sliced samples) and the host wood.

For the cactus analyses, statistical analyses were used to test whether the data from the same experimental groups distributed among several plants could be pooled (**Article A**, **Article D**, and **Manuscript A**). Furthermore, statistical tests were performed to test for significant differences between the various analyzed groups. In **Article A**, statistical tests were used to test whether the mechanical healing effect (HE_{21}) differed significantly from 0.

For the selection of the appropriate statistical tests in each study, the data of the individual groups were tested for their normal distribution and their variance homogeneity. All statistical analyses were performed using GNU R (version 3.2.3 to 4.1.2). Detailed information concerning the statistical tests, post-hoc tests, significance levels, and the packages used can be found in the respective article or manuscript.

4 SUMMARY OF RESULTS AND DISCUSSION

4.1 Mistletoe-host connection

In order to analyze the underlying structures of the life-long damage-resistant mistletoe-host connection, interfaces were morphometrically characterized at several ages of the mistletoe and visualized at tissue and cellular levels. The results can be found in the following chapter and in **Article C**. The mechanical characterization of the connection under tensile loading, likewise taking into account the age of the mistletoe, are summarized in **chapter 4.1.2** and in **Article E**.

4.1.1 Morphology and anatomy of the mistletoe inside the host

The 130 mistletoes analyzed ranged from 3 to 21 years, with 15 juvenile plants (3 to 6 years), 88 female plants (6 to 19 years), and 27 male plants (6 to 21 years). The female bias of 76.5% was within the range for *V. album* measured by BARLOW *et al*. (1978) in Europe (72.9 to 76.5%) and by SHOWLER (1974) per seedling experiments (67.3%). The female bias in mistletoes is assumed to be determined by genetic factors rather than environmental influences (WIENS *et al*., 1996). The extent of the host branch hypertrophy did not correlate with mistletoe age and had a median value of 42% (IQR: 38%), but could be as high as 242% for thin host branches (an overview of all analyzed morphological variables and their correlation with mistletoe age can be found **Table 1** in **Article C**).

The µCT scan of the 4-year-old mistletoe with tissue segmentation revealed that the endophyte had spread more than 5 cm along the host branch at this young age (**Figure 13D**). The number of wedge-shaped sinkers was greatest (five) near the penetration site, and they extended furthest toward the pith of the host branch. Acropetally and basipetally, the number of individual sinkers and their respective sizes successively decreased (compare upper and lower box in **Figure 13**). This allows the mistletoe not only to prime the outgrowth of adventive shoots in the early stages, but above all to enlarge the interface with its host in order to take up sufficient amounts of water and dissolved nutrient salts (YOSHIDA *et al*., 2016; TEIXEIRA-COSTA, 2021) and to ensure mechanical anchorage.

The performance of µCT data segmentation supported with stereomicroscopic images of the cross sections (**Figure 13A**&**B**) allowed the segmentation of the entire endophyte (sinkers and cortical strands) of the mistletoe with a single sample and scan (**Figure 13C**&**D**). This had

the advantage that no contrast agents were needed to highlight individual tissues, a step that would have required multiple samples and scans to adequately visualize all tissues (TEIXEIRA-COSTA & CECCANTINI, 2016). The stacking of stained microscopic sections provides cellular resolution of the endophyte but can only be performed on small samples (several millimeters) and is destructive and time costly (HESSE *et al*., 2019; MASUMOTO *et al*., 2021).

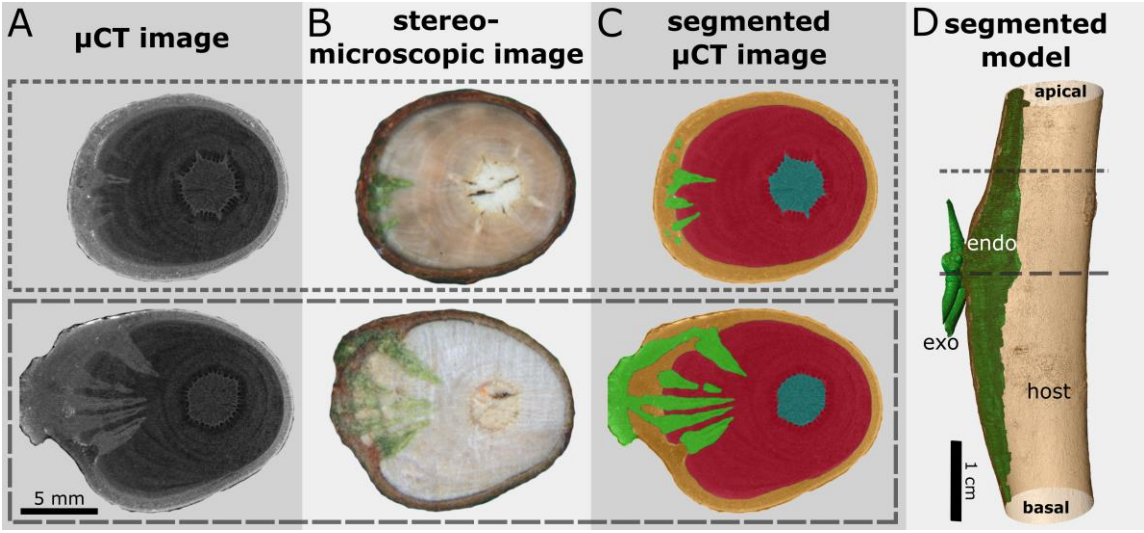

Figure 13: Tissue segmentation (**C**) of the µCT scan (**A**) of a 4-year-old European mistletoe and its host branch supported by steromicroscopic images (**B**). Mistletoe tissues are colored green, host bark brown, pith gray, and wood red (**C**). In the model (**D**), the truncated exophyte (exo) and endophyte (endo) are labeled. For (**A**-**C**), two exemplary transverse sections through the host branch are presented, located apical to the mistletoe penetration site (dotted lines, upper block) and directly through it (dashed lines; lower block). Adapted from **Article C.**

During the joint, but also competitive growth of the mistletoe and its host, several thin sinkers of the young mistletoe (**Figure 14A**&**B**) continuously merged into a large main sinker (**Figure 14C**-**F**). At the same time, this main sinker grew basally and apically of the penetration site, resulting in a cone shape (**Figure 14E**&**F**).

The large main sinker can presumably mechanically withstand the growth of the host and the resulting internal stresses better than the individual thin sinkers. This acclimatization within the mistletoe's lifetime prevents the loss of the physiological and mechanical connection between mistletoe and host, which would lead to the death of the mistletoe.

A clear dividing line between the mistletoe and host was apparent on a cellular level at all ages (**Figure 15A**-**D**). However, no breakdown of cell-walls, as described by SMITH & GLEDHILL (1983), was observed. Vascular elements ran within the mistletoe sinker and diverged from this point to form physiological connections (see the perforation plates in **Figure 15C**) with the host at their interface.

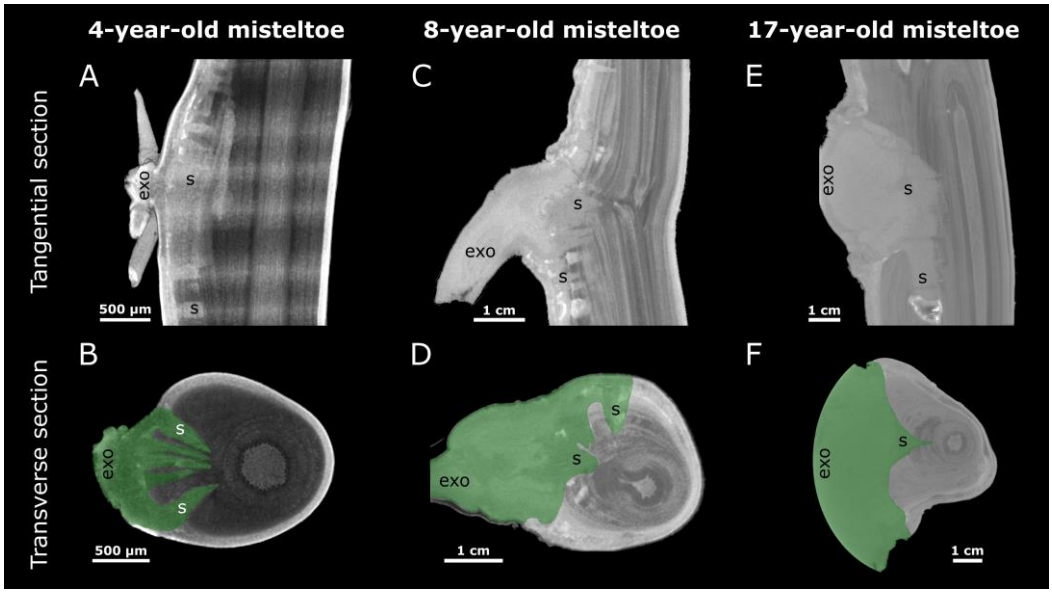

Figure 14: Comparative µCT analyses of a young (4 years; **A**&**B**), middle-aged (8 years; **C**&**D**), and old (17 years; **E**&**F**) European mistletoe, with the sinker (s) and exophyte (exo) labeled. A tangential section and the transverse section through the penetration site (with the mistletoe tissue marked in green) are presented for each sample. Adapted from **Article C.**

Thickened cell walls (**Figure 15B**) and lignin inclusions (**Figure 15E**&**F**) were frequent near this interface. These gradually diminished toward the middle of the sinker, which consisted predominantly of less rigid parenchyma cells. This led to a gradual transition of the mechanical properties of the two species. In addition, misoriented host cells had fused into swirls near some interfaces, indicating the competition and resulting stresses for available space during joint and competitive growth (**Figure 15D**).

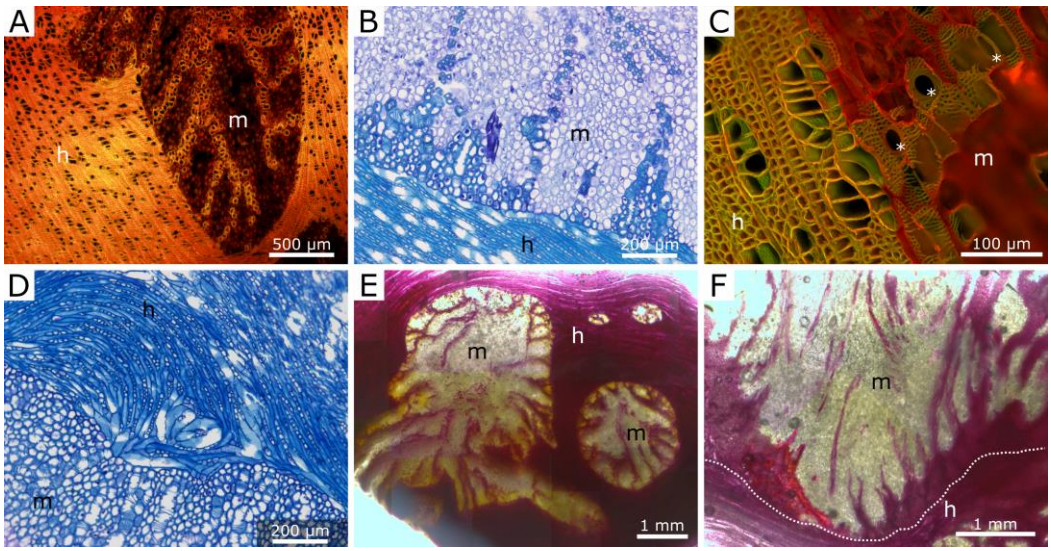

Figure 15: Light microscopic images of the interface (dotted line in **F**) between the European mistletoe (m) and its host (h), stained with acridine orange (**A**&**C**), toluidine blue (**B**&**D**), and phloroglucinol (**E**&**F**). The asterisks in (**C**) mark the perforation plates of the mistletoe vessel elements through which most of the water uptake is accomplished. Adapted from **Article C.**

4.1.2 Biomechanics of the mistletoe-host connection

The mechanical properties of the mistletoe-host connection were characterized by tensile tests to failure on intact samples or sliced samples from the attachment site. Of the 70 tested samples, 33 failed between the clamps, and in the other 37 samples, failure ran at least partially along the clamps. In all but two samples (with failure exclusively through mistletoe branch), failure ran at least partially along the interface between the host and mistletoe.

A single force peak with a subsequent force drop was found for the force-displacement curves of the sliced samples (**Figure 16B**), whereas pre- and post-failure events were observed for most of the intact samples (**Figure 16A**). These were presumably caused by the successive failure of individual sinkers. This redundancy of the sinkers, especially in young mistletoes, implies that a partial physiological and structural loss is tolerated to preserve the (multi-)functionality of the overall system. A similar benign failure can be found for the successive (pre-)failure events of the adhesive pads of Boston ivy (STEINBRECHER *et al.*, 2010; ROWE & SPECK, 2015). In order to analyze the behavior of the interface of single sinkers and the entire system under tensile load, *in situ* tensile tests with simultaneous 3D imaging could be performed in follow-up experiments.

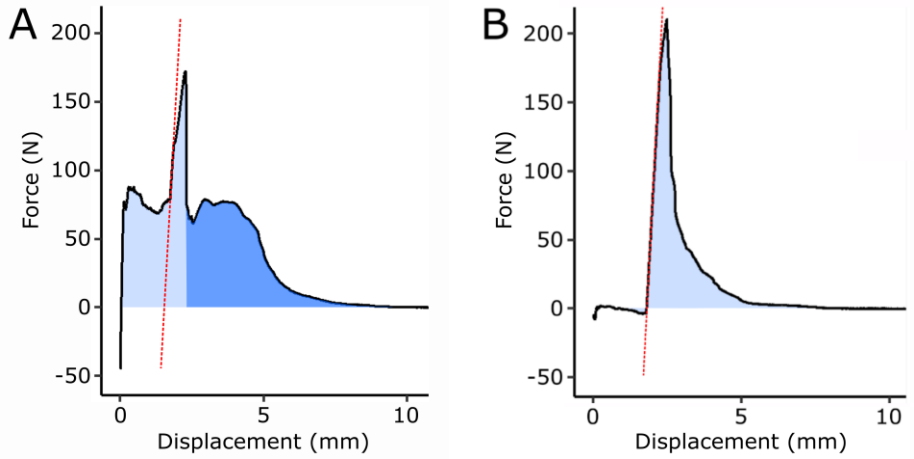

Figure 16: Examples of force-displacement curves of intact (**A**) and sliced (**B**) mistletoe host samples under tensile loading. The slope of the linear part of the main peak (red dashed line) and the integral of the curve (blue; the intact sample pre- (light blue) and post-failure (dark blue) regions are distinguished) are marked. Adapted from **Article E.**

The rough fracture area A_r, corresponding fracture area A_c, maximum force F_{max}, and work of fracture W showed a positive correlation with the age of the mistletoe for at least one of the sub-groups (divided by intact and sliced samples, and by failure at the interface or at the clamp). This can be explained by the mere growth of mistletoe and the resulting increase in

the size of the attachment site with the host. The roughness *R*, tensile strength σ_{max}, fracture energy E_f, and strain at failure ε_f were not age-dependent (all correlation *p*-values > 0.05), which indicates that the failure-resistant connection between mistletoe and host is established at a young age and does not diminish over the course of joint growth.

The median roughness of the failure surface of the mistletoe-host samples was significantly larger by 22% to 55% compared with that of the host wood samples tested along the same fiber orientation. Because of the high dependence on the spatial resolution of the measurement device, the comparability of the roughness values is, however, limited to samples measured with the same equipment and settings (compare e.g., MOREL *et al*., 1998; BÜHRIG-POLACZEK *et al*., 2016).

The values of tensile strength of the mistletoe-host connections calculated on the rough fracture surface were about a factor of three (for sliced samples) to a factor of five (for intact samples) lower than those for the host wood samples, with significant differences also being observed between the two mistletoe groups (**Figure 17A**). No significant difference between the intact and sliced samples was found for fracture energy calculated on the rough fracture surface. Median values for the mistletoe samples were about 50% lower compared with those for the host wood samples (**Figure 17B**). The diminished difference between the three groups for fracture energy compared with tensile strength can be explained by the pre- and post-failure events of the intact samples; these prolong the stress-strain curves and thus enlarge the area under the curve (**Figure 16**). This illustrates how important the various sinkers and their redundancy are for the structural integrity of the entire mistletoe-host junction, particularly at a young age of the mistletoe.

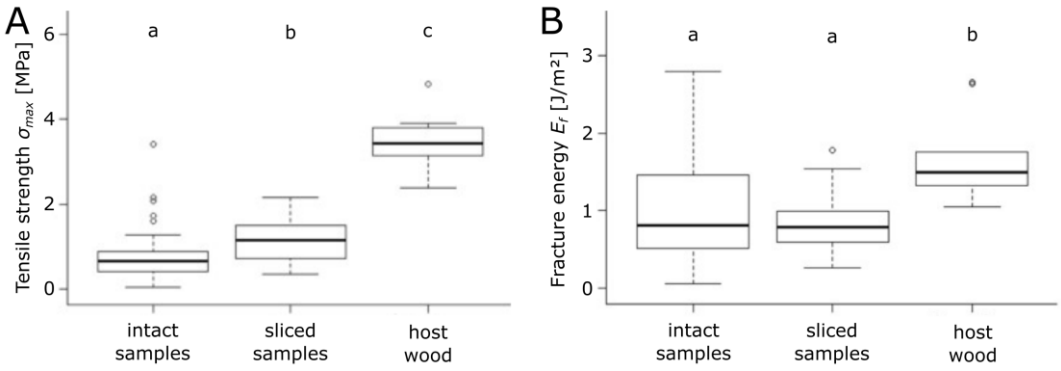

Figure 17: Boxplots of tensile strength σ_{max} (**A**) and failure energy E_f (**B**) (both normalized on rough fracture area A_r) under tensile load of intact (*N* = 39) and sliced (*N* = 31) mistletoe-host samples and of host wood samples tested normal to grain (*N* = 9). Similar small letters indicate groups without significant differences.

Scatterplots of the age-dependent variables can be found in **Figure 6** of **Article E**, a detailed overview of all analyzed age-independent mechanical variables in **Table 1** of **Article E**, and detailed statistics in Supplement **Tables S1** & **S2** of **Article E**.

The energy required to propagate a crack depends on the relative extent of the non-linear range of the force-displacement curve to the total curve. The larger that this proportion is, the more energy is required for crack propagation, and the larger is the resulting fracture area of the samples (resulting in a larger roughness), e.g., attributable to torn-out fibers (NIKLAS, 1992; BEISMANN *et al.*, 2000). This effect is visible in the force-displacement curves of the intact sample with larger non-linear parts (**Figure 16**) and in the increased roughness for the intact samples (**Table 1** in **Article E**).

The local strain analyses revealed that the largest strains occur under tensile loading along the mistletoe-host interface (**Figure 18**). Strain values of about 30% led to crack initiation along the mistletoe-host interface (in some samples, slightly shifted toward the inner part of the sinker) (asterisk in **Figure 18C**).

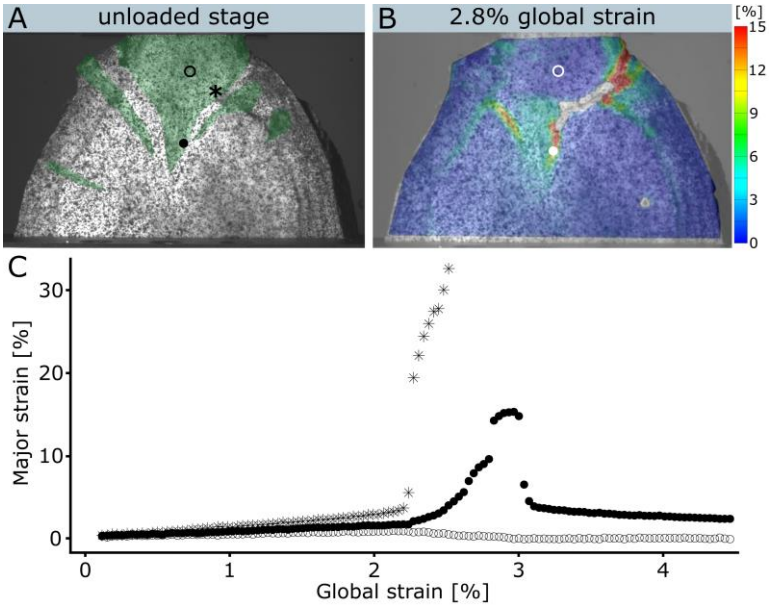

Figure 18: Local surface strain analysis by using digital image correlation (DIC) of a sliced mistletoe-host sample under tensile load. (**A**) A sprayed speckle pattern was applied to increase surface contrast in unloaded stage. The mistletoe sinkers of the sample are colored in transparent green. Three points were selected for detailed analysis: open circle at the sinker base, asterisk at the mistletoe-host interface, and filled circle at the tip of the sinker. (**B**) The strain pattern shortly after the crack developed (at 2.8% global strain). (**C**) shows the local strains of the three single points marked in (**A**&**B**) over the entire tensile test. Adapted from **Article E**.

The fracture propagated either along the interface or, depending on the angle of the interface to the load, additionally through the host wood and/or the mistletoe sinker (See

Figure 8 in **Article E** for DIC analysis of additional samples). If the sinker tip remained in the host wood, local strains did not decrease to zero after failure, indicating plastic deformations within the tissue (filled circles in **Figure 18C**). Almost no strains occurred inside the main sinker (open circles in **Figure 18C**). The results show that the interface between mistletoe and host is subject to the largest strains under tensile load, making the gradual transition of lignification and cells with thickened cell walls (**Figure 15**) at this site particularly important, and that redundancy of individual sinkers, especially in young mistletoe, can play an important role in preventing complete failure of the connection.

4.2 Damage management in cacti

The results of the morphological, anatomical, and biomechanical self-repair analyses of the cactus branches are presented in the following chapter and in **Article A**. The comparative analyses of the abscission (and stiffening) of the branch-branch junctions are divided into a study of their morphology and anatomy (**Chapter 4.2.2.1** and **Article D**) and a study of the biomechanical properties of the entire junction and the tissues involved (**Chapter 4.2.2.2**, **Article D**, and **Manuscript A**).

4.2.1 Self-repair of cacti branches

Macroscopic observations of the cactus branches after artificial ring injury revealed that the wound edges of *O. ficus-indica* initially remained in contact before a slight rolling in became visible after a few days. However, this movement was less pronounced than in *Delosperma cooperi* (KONRAD *et al.*, 2013) or in succulent plants with cylindrical organs (ANANDAN *et al.*, 2018) in which tensile pre-stresses of the outer tissue layers lead to almost complete closure of the wound after longitudinal wounding. After one week, a wound gap became visible, together with the occurrence of the death of surrounding cell layers (white discoloration). In *C. bigelovii*, the wound gap was visible immediately after wounding and widened over the next few weeks, with dead tissue being present around the wound (**Figure 1** in **Article A**).

The anatomical analyses revealed that the ring incision severed the epidermis, the underlying hypodermis, and large portions of the cortex parenchyma (**Figure 19A**&**D**). In both species, the formation of a suberized layer of parenchyma cells around the wound occurred after about three days (**Figure 19B**&**E**; also regularly found in abscission zones; ADDICOTT, 1982). Over the next days and weeks, a wound periderm grew that completely

closed the wounds, with a rather fragile connection to the underlying (partially newly formed) parenchyma (**Figure 19C**&**F**). Sealing by oozing mucilage was not observed in any of the analyzed samples.

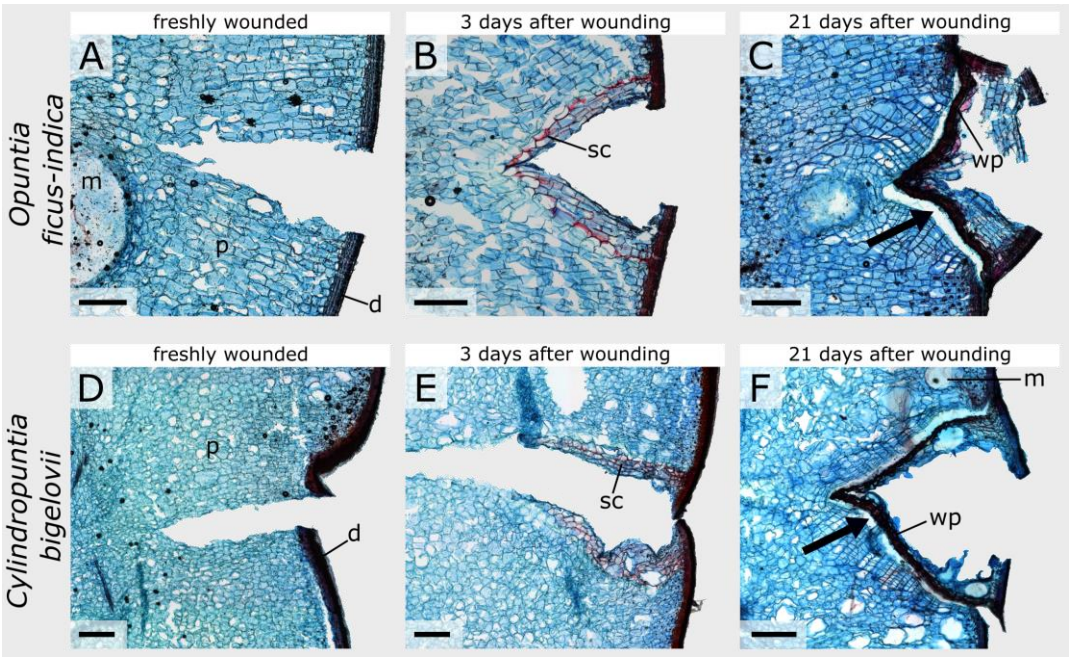

Figure 19: Anatomical overview of the repair processes of *Opuntia ficus-indica* (**A**-**C**) and *Cylindropuntia bigelovii* (**D**-**F**) branches. Tangential sections stained with tolouidine blue immediately after artificial wounding (**A**&**D**), and a healing period of 3 days (**B**&**E**) and 21 days (**C**&**F**). The wounding extends through the dermal tissue (d; consisting of epidermis and hypodermis) and portions of the parenchymal tissue (p) in which large mucilage cells or channels (m) are frequently found. Cellulose-containing cell walls are stained blue, lingo-suberinized cell walls are stained red. In the first few days after wounding, a suberin layer (sc) seals the wound, before a multilayer wound periderm (wp) forms after 2-3 weeks. During section preparation, the periderm often detached from the underlying newly formed parenchyma (black arrows). All scale bars equal 500 µm. Adapted from **Article A.**

The wounding effect W_0 after artificial ring incision for all three mechanical analyzed variables (bending stiffness of the first and second range and work) ranged between 18.4% and 26.4% for *O. ficus-indica* and between 21.1% and 36.2% for *C. bigelovii*. After a healing period of 21 days, *C. bigelovii* showed significant positive healing effects HE_{21} only for the bending stiffness of the second linear range (between 8.7% and 9.5%). No significant positive healing effects were observed for *O. ficus-indica*, and for one of the two plants studied, the values of the healing effect of all three variables were found to be significantly negative (between -19.0% and -31.2%). This further decrease in mechanical performance during the healing phase can be explained by the death of tissues and by the periderm, which seals the wound but is mechanically only weakly attached to the surrounding tissue (arrows in **Figure 19C**&**F**).

NOBEL & MEYER (1991) showed, with their bending tests on *O. ficus-indica*, that the stiffness of the branches is at least twice as high as that of the junctions. The presented mechanical values suggest the difference in stiffness between the branch and junction is even larger for *C. bigelovii* (**Chapter 4.2.2.2**; **Article D**, and **Manuscript A**). Thus, even if the mechanical properties were reduced between 18 and 36%, the branches would still not be the most fragile part of the plant. A rapid and complete sealing to minimize water loss and to avoid pathogen attack seems to be of greater ecological benefit to the plant than complete regeneration of its mechanical properties, so that the principle of 'sufficient is good enough' applies.

4.2.2 Abscission of cacti branches

4.2.2.1 Morphology and Anatomy of cacti junctions

No significant difference was found between the maximum cross-sectional area of lateral branches of *O. ficus-indica* and *C. bigelovii*. However, the area of lateral junction (by 62.3%) and the area ratio (by 78.9%) of *O. ficus-indica* were significantly larger than those of *C. bigelovii* (**Table 1**). The marked tapering of the lateral branches to an area of about 4% and 7% at the junction illustrates that these are the clear morphological weak points of the analyzed Opuntioideae. The lower absolute and relative values of the junction area make this particularly evident for *C. bigelovii*. More detailed morphometric analyses of the branches and junctions, including the axial second moment of area and torsion constant, can be found in **Table 1** of **Article D**.

Table 1: Morphometric data of junction area, maximum branch cross-sectional area, and the ratio of the two values for *Opuntia ficus-indica* and *Cylindropuntia bigelovii*. The mechanical values are given as the median (interquartile range). If a normal distribution and equal variances were obtained, then the Welch two-sample *t*-test ([a]) was used for statistical analysis; otherwise, the Wilcoxon rank sum test ([b]) was used. Adapted from **Article D**.

	O. ficus-indica	***C. bigelovii***	**Statistical difference *p*-value**
Sample size *N*	12	12	
Junction area [mm²]	25.0 (15.1)	15.4 (7.2)	0.0068 [a]
Maximum branch area [mm²]	382.1 (138.0)	395.6 (103.4)	0.4713 [a]
Area ratio [/]	0.068 (0.040)	0.038 (0.012)	0.0011 [b]

The 3D visualizations of the outer shape of the cacti branches using MRI reflected those features visible to the naked eye: flat branches with slight curvatures at the areoles for *O. ficus-indica* and cylindrical branches with undulating areoles for *C. bigelovii* (**Figure 20A**&**C**), both capable of a volume increase through water uptake with a constant surface area (MAUSETH, 2006). The course of the vascular bundles in both species was net-like in the branch, with a distinction between the main bundles and secondary bundles in *O. ficus-indica* and individual bundles emerging from the net to supply the areoles in *C. bigelovii*. Within the branch-branch junctions, the vascular bundles of both species converged to form an almost enclosed circle, which reverted, apical of the junction, to the net-like structure (**Figure 20B**&**D**). In the junctions of *O. ficus-indica*, a ring-shaped collar consisting of peridermal tissue covered large parts of the epidermis. In one of the segmented samples, the periderm coverage extended over parts of the lateral branch near the junction (**Figure 20A**). No periderm accumulation was found in the analyzed junctions of *C. bigelovii*. The periderm deposition reduces the gas exchange and photosynthetic activity of green branches. Therefore, it is crucial for the survival of the plant that this is a gradual process that does not cover the surface of all young branches (NOBEL, 2002). In the older stages, a successive accumulation of periderm layers, spreading from the junctions over the branch surfaces, contributes to the increasing demand for structural stability.

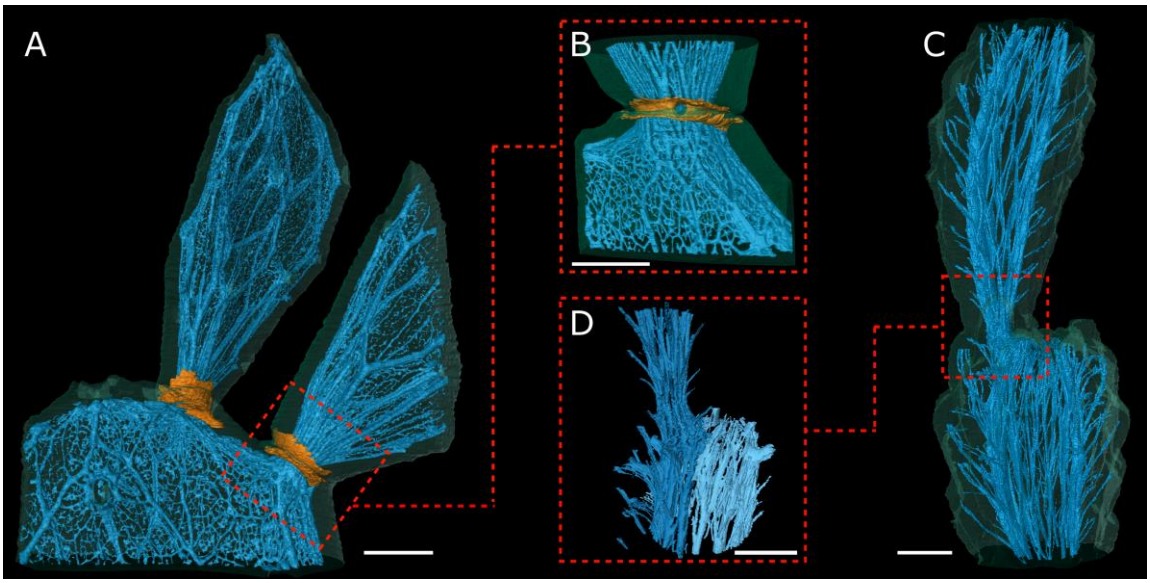

Figure 20: Segmented magnetic resonance scans of lateral branches and junctions of *Opuntia ficus-indica* (**A**&**B**) and *Cylindropuntia bigelovii* (**C**&**D**). The epidermis is depicted in transparent green, with the vascular bundles in blue, in (**D**) distinguishing whether they pass through the junction (light blue) or terminate in a dormant bud (dark blue); the periderm is shown in orange. All scale bars equal 1 cm. Adapted from **Article D**.

Light microscopic images of stained sections through the junctions revealed that the periderm overlay in *O. ficus-indica* consisted of densely packed phellem cells, a single meristematic phellogen layer, and multiple layers of thin-walled phelloderm (**Figure 21B)**. The parenchyma tissue of both species gradually changed from wide-lumen cells in the branches to small-lumen cells with thickened cell walls in the junction (**Figure 21A**&**C**). This transition to the small-lumened parenchyma cells resembles the abscission zones, although these usually consist of only a few cell layers (ADDICOTT, 1982). Together with the ability to form a wound periderm to seal exposed tissues (**Chapter 4.2.1**; 'protective layer'), one can assume an abscission of the (lateral) branches in the two examined cacti species, even though a hormonal influence plays no or only a minor role in the mechanically controlled shedding of the branches (biochemical studies on this were not part of the present work).

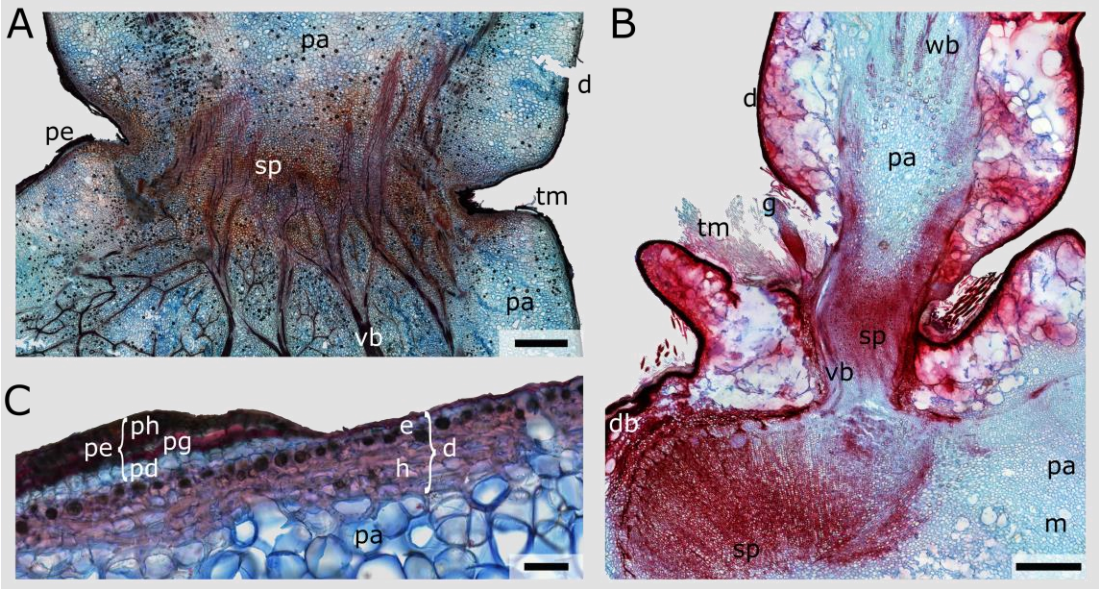

Figure 21: Stained light microscopic sections through the junctions of *Opuntia ficus-indica* (**A**) and *C. bigelovii* (**B**), with a detailed view of the periderm tissue of *O. ficus-indica* (**C**). Branch parenchyma (pa) with thin cell walls converts to small-volumed parenchyma with thickened cell walls (sp) at the junction site. Vascular bundles (vb) run embedded in the parenchyma, with wide band tracheids (wb) being found mainly in *C. bigelovii*. The dermal tissue (d), consisting of an epidermis (e) and hypodermis (h), of *O. ficus-indica* at the junction is covered by a periderm (pe) consisting of phellem (ph), a single layer of meristematic phellogen (pg), and phelloderm (pd). Trichomes (tm) and glochids (g) grow in the notch of the junctions. A dormant bud (db) and mucilage cells (m) are present in the sample of *C. bigelovii*. Scale bars equal 2 mm in (**A**&**B**) and 100 µm in (**C**). Adapted from **Article D.**

Because of the extremely high mucilage content in the samples and the large mechanical differences between the dermal tissue and large-lumen parenchyma, fully intact sections of *C. bigelovii* were difficult to prepare, despite various embedding and cutting techniques having been tried.

A detailed histological illustration of the junctions and tissues involved, and a transverse serial section through a junction of *O. ficus-indica*, revealing the outgrowth of a lateral branch from an areole and the resulting periderm growth, can be found in **Figures 5**-**7** of **Article D**.

4.2.2.2 Mechanics of cacti junctions

The tensile tests of the individual tissues showed that a peridermal coverage on the dermal tissue (epidermis and hypodermis) of *O. ficus-indica*, although only increasing its thickness by about 20%, increased its median strength by about threefold, exceeding that of the dermal tissue of *C. bigelovii* by about 50%. The resulting stiffening is indicated by a reduction in the deformation at break median from 17.2 to 4.5%, and the simultaneous approximately tenfold increase in the elastic modulus (median values from 44.1 to 464.0 MPa; in good agreement with the values for the dermal tissue of the climbing cactus *Selenicereus setaceus* obtained by BASTOLA *et al*. (2021)). A continuous periderm layer was not found in *C. bigelovii*, either in the junction or in more basal branches of the experimental plants, indicating that the stiffening of the junctions occurs delayed at much later stages in this species.

Even larger differences were found between the mechanical properties of the vascular bundles of *O. ficus-indica* (where no significant differences were found between the young and the older samples) and those of *C. bigelovii*: median tensile stiffness was about 200 times higher, median tensile strength was about 25 times higher, and median fracture energy was higher by a factor of over 15 in *O. ficus-indica*. In contrast, the fibers of *C. bigelovii* failed at about five times higher strain values (**Table 2**). Additional mechanical variables of the tissues, a comparison between the longitudinally and transversely collected samples in *O. ficus-indica*, and the statistical analysis of the data can be found in **Article D**.

The young junctions of *O. ficus-indica* and those of *C. bigelovii* did not differ significantly in their cross-sectional area and the mass of the lateral branch and thus represented readily comparable groups. However, the median maximum force (51.2 N to 14.4 N) and the median tensile stiffness (19.0 N/mm to 15.8 N/mm) were significantly higher in the young branches of *O. ficus-indica*, although these were, in turn, by a factor of three lower than those of the old branches (153.0 N and 40.4 N/mm). For all three groups, a medium to strong positive

linear correlation (Pearson's ρ > 0.5) of maximum force and tensile stiffness with lateral branch mass was found (**Table 1**&**2** and **Figure 7** of **Manuscript A**).

Table 2: Mechanical data of the dermal tissue (for *Opuntia ficus-indica* cut in a longitudinal branch direction), the vascular bundles, and the entire branch-branch junction of young and older *O. ficus-indica*s samples and *Cylindropuntia bigelovii* samples. The mechanical values are given as median (interquartile range). For values marked with an asterisk, the data of the two test plants differ significantly but are presented pooled for better clarity. A detailed overview of the presented and further mechanical variables, including statistical analysis, can be found in **Article D** for single tissues and in **Manuscript A** for entire junctions.

Sample	Tissue or organ tested	Sample size *N*	Elastic modulus [MPa]	Tensile strength [MPa]	Fracture energy [mJ/mm²]	Deformation at break [%]
***Opuntia ficus-indica* (young)**	**dermal tissue**	12	44.1 (13.7)	4.1 (0.86)	11.9 (2.7)	17.2 (3.41)
	vascular bundle	12	1233.8 (1061.8)	56.2 (56.5)	36.2 (48.8)	10.9 (7.4)
	junction	14	45.5 (20.6)	3.8 (0.6)	18.2 (10.8)	25.0 (5.6)
***Opuntia ficus-indica* (older)**	**dermal tissue (periderm coverage)**	12	464.0 (179.5)	*11.4 (3.7)	4.8 (4.1)	4.5 (2.3)
	vascular bundle	12	1674.0 (384.5)	55.1 (35.8)	41.9 (63.0)	*9.7 (6.0)
	junction	14	23.7 (11.1)	2.7 (0.5)	19.9 (8.8)	28.2 (8.5)
Cylindropuntia bigelovii	**dermal tissue**	12	*54.5 (37.8)	*7.2 (4.1)	3.3 (1.8)	19.5 (8.8)
	vascular bundle	12	7.4 (2.9)	2.1 (1.3)	2.3 (1.6)	*53.4 (28.4)
	junction	15	15.8 (6.2)	1.4 (0.2)	4.1 (2.0)	12.6 (4.7)

After normalization of the data, the values for elastic modulus and tensile strength were highest for the young junctions of *O. ficus-indica*, intermediate for the older junctions of *O. ficus-indica*, and lowest for *C. bigelovii*. However, we found no significant difference in fracture energy between the young and older samples of *O. ficus-indica*, which can be explained by an elongated stress-strain curve for the older samples. The lowest fracture energy values were found for *C. bigelovii*. Similarly, no significant differences were found for the deformation at break values between the two groups of *O. ficus-indica*, each being about twice as high as the median values for *C. bigelovii* (**Table 2**).

Since the tensile modulus of the epidermis markedly increases through periderm formation but the (effective) tensile modulus of the older junctions of *O. ficus-indica* is only about half that of the younger junctions, an allometry of the involved tissues during growth can be assumed (NIKLAS, 1994; SHINGLETON, 2010; KAMINSKI *et al.*, 2017). This means that the relative

cross-sectional proportion of non-lignified parenchyma increases, whereas the relative proportion of the dermal tissue (and assumingly the vascular bundles) decreases. Thus, in addition to the (absolute) stiffening of the lateral junctions of *O. ficus-indica*, there is an increase in water storage capacity resulting from the increase in parenchyma cells.

Local surface strains of all three species showed the highest values around the junction, resulting in losses of pattern detection of the digital image correlation in this region. In the two samples of *O. ficus-indica*, but not in the sample of *C. bigelovii*, strain of about 5 to 8% was found in the branch surfaces, which shows that the branches are more involved in taking up tensile forces than is the case in *C. bigelovii* (**Figure 22A**-**C**).The junction strain value increased about equally with the sample strain for the samples of the three groups, but failed already at about 70% for the sample of *C. bigelovii*, while the samples of *O. ficus-indica* failed at 180% (young junction) and 220% (older junction). All samples showed a sudden failure (steep increase of junction strain values after failure), which in the older junction of *O. ficus-indica* was preceded by a pre-failure event (visible by the kink at the end of the gray curve) (**Figure 22D** and **Figure 8** of **Manuscript A** with additional section analysis).

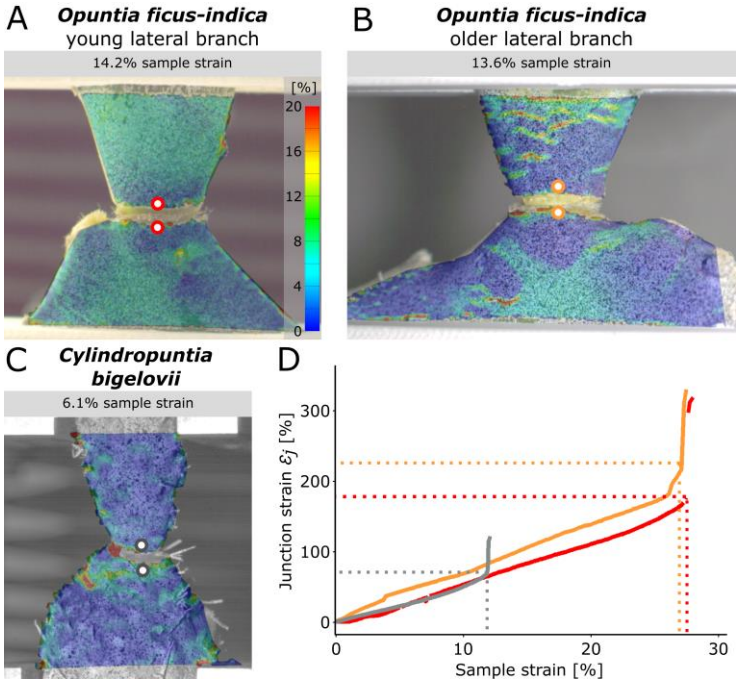

Figure 22: Local surface strains of lateral junctions of a young (**A**) and an older (**B**) *Opuntia ficus-indica* sample and of a *Cylindropuntia bigelovii* sample (**C**) under tensile load (at about half sample strain to failure). The strain scale in (**A**) applies to all three samples and indicates the value of the major strain. (**D**) shows the junction strains (calculated from the distance between the two points at the junction) over the strain of the entire sample, with the red curve relating to the young and the orange curve to the older sample of *O. ficus-indica* and the gray curve to the sample of *C. bigelovii*. The dotted colored lines indicate the respective axis intercept. Adapted from **Manuscript A.**

Comparison of the failure site and surface revealed a change from predominant failure directly at the junction with smooth fracture surface in young samples of *O. ficus-indica* to an increasing proportion of failure through the branches with fibrous fracture sites in the older samples. In *C. bigelvii*, most samples failed at the junction, with parts of a branch pulled out, resulting in a cup and cone fracture surface (**Table 3**). The proportions of the three sections (elastic, plastic, and failure) of the entire stress-strain curve also differed between the three groups: while plastic deformation predominated in the young junctions of *O. ficus-indica*, failure accounted for the largest proportion in the older junctions (which accounted for only about 4% in the young samples). For *C. bigel*ovii, the plastic portion also accounts for the largest proportion (**Table 3**).

Table 3: Failure characteristics of the lateral branch-branch junction of *Opuntia ficus-indica* (young and older samples) and *Cylindropuntia bigelovii* under tensile loading. The relative proportion of the fracture site (and the resulting fracture surface), the total strain to failure, and the relative proportion of the elastic, plastic, and failure ranges thereof are presented. The highest value of each group is indicated in bold. Adapted from **Manuscript A**.

	Sample	***Opuntia ficus-indica*** **young**	***Opuntia ficus-indica*** **older**	***Cylindropuntia bigelovii***
	Sample size *N*	14	14	15
Proportion of fracture site (& surface)	**junction (smooth)**	**93%**	22%	20%
	junction & branch (cup & cone)	7%	14%	**80%**
	branch (rough)	/	**64%**	/
Proportion of total strain	**Total strain [/]**	0.25	0.48	0.18
	Elastic range	20.2%	11.7%	17.1%
	Plastic range	**74.5%**	44.8%	**49.0%**
	Fracture range	4.4%	**47.2%**	27.5%

Because of the relatively complex geometry of the junctions and the intergrowth of its tissues, it is not possible to simply sum up the mechanical properties (and their relative contribution to the overall structure) of the tissues involved (compare **Article D**), in order to obtain the mechanical properties of the overall junction. **Figure 9** provides a schematic overview of the junction tissues and the effect of the notch on the mechanical behavior of the junction. Not all tissues are equally stressed under tensional loading and a stress gradient

is generated within the junctions, because their diameter is smaller compared to that of the adjacent branches (**Figure 9A**). **Figure 9B** shows that a transverse compression of the junctions occurs in addition to the longitudinal stretching of the sample (according to their Poisson's ratio; purple arrows). A periderm support around the notch (gray area) counteracts these effects (pink arrows), and thus reduces the forces acting on the junction. This can explain why the proportion of samples that fail through the branch and not at the junction increases for the older junctions of *O. ficus-indica*. Another illustration of this effect is provided by the local strain analyses, where lower strain values were found around the older junction of *O. ficus-indica* compared to the apical and basal part of the adjacent branches (**Figure 22 B**). The sketched arrangement of the main tissues in **Figure 9C** shows that the epidermis first unfolds under tensile loading, whereas the net-like vascular bundles can take up forces immediately (although it should be noted that, depending on the angle and direction of growth, these must first align themselves along the forces applied). This illustrates that an unambiguous assignment of the tissues and their contribution to the uptake of stresses during the course of tensile loading up to failure is not given.

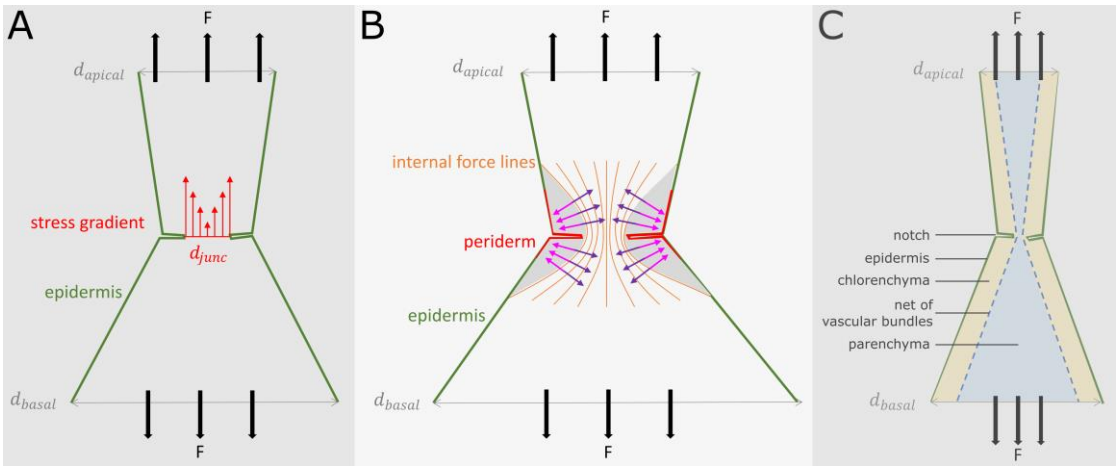

Figure 23: Schematic representation of the junctions of the three cactus groups studied, each illustrating a different aspect of the notch effect. In (**A**), the model of a young lateral branch junction of *Opuntia ficus-indica* shows a stress gradient (red arrows) caused by the diameter at the junction being smaller than the diameter in the branch at which the tensile forces act. In (**B**), the model of an older junction of *O. ficus-indica* shows the effect of stiffening by the periderm support. The junction shows transverse contraction (according to Poisson's ratio; purple arrows) together with longitudinal elongation. At the same time, however, the gray marked parts are not (or at least less) stretched due to the stiffening, generating an outward transverse force that prevents transverse stretching in this area (after 'Kerbwirkung' by Ralf Pfeifer, licensed under CC BY-SA 3.0, available under https://commons.wikimedia.org/wiki/File:Kerbwirkung.svg). In (**C**), the model of a junction of *Cylindropuntia bigelovii* reveals the basic structure and distribution of the five tissue layers. Under tensile loads, the epidermis initially unfolds in the notch area and the network of vascular bundles stretches and takes up the initial forces. Adapted from **Manuscript A.**

In summary, although the mechanical properties of the young lateral junctions of *O. ficus-indica* are higher than those of the junctions of *C. bigelovii*, they fail at rather low forces and their lateral branches can also serve as offshoots for vegetative propagation (EVANS *et al.*, 2004). However, already in a young stage, the plant allocates a large amount of resources to the lateral branches (e.g., growth and water storage). This is accompanied by earlier growth and structural strengthening of the junction compared those of *C. bigelovii*, making them less susceptible to mechanical failure. An overview of the morphometric, morphological, anatomical, and biomechanical characteristics of the two cactus species, with particular respect to their lateral branch-branch junctions, is presented in **Figure 4**.

Table 4: Overview of the similarities and dissimilarities comparing various features of *Opuntia ficus-indica* and *Cylindropuntia bigelovii* with focus on their (lateral) branch-branch junctions. Adapted from **Article D** and **Manuscript A**.

	Opuntia ficus-indica	***Cylindropuntia bigelovii***
	Life-form	
Growth-form	stem succulent tree-like	shrubby
Main propagation	sexual via fruits/seeds	vegetative via shed offshoots
(lateral) branch junction stability	fragile in young lateral junctions and stable in older junctions	fragile (abscission)
	Similarities	
Morphometry	distinct cross-sectional taper towards the junctions with comparable junction area (for young lateral junctions of *O. ficus-indica*)	
Morphology	net-like arrangement of vascular bundles that close together circularly within the junctions	
Anatomy	changes of tissue characteristics from the branches to the junctions: lumen of parenchyma changes from large to small and the amount of wide-band tracheids changes to a smaller number	
Mechanical properties	comparable stiffness of the dermal tissues (without periderm coverage); comparable effective tensile modulus between junctions of *C. bigelovii* and older junctions of *O. ficus-indica*	
	Dissimilarities	
Morphometry	*C. bigelovii:* significantly lower absolute and relative junction cross-sectional areas	
Morphology	*O. ficus-indica:* periderm formation around lateral junctions	
Anatomy	*O. ficus-indica:* periderm formed as wound tissue by outgrowing areoles	
Mechanical properties	*O. ficus-indica:* periderm stiffens dermal tissue by a factor of about 10 *O. ficus-indica:* strength and stiffness of vascular fibres are higher by a factor of about 25 and 200 *O. ficus-indica*: effective tensile modulus (only for young junctions), maximum force, tensile strength, fracture energy, and strain at fracture of junctions are significantly higher	

A comparison of the force-displacement curves of different failure modes, detailed correlation analyses of the mechanical variables with the apical branch mass, and finite element (FE) simulations of the elastic behavior of the junctions based on multi-material shell models and the mechanical properties of the analyzed tissue can be found in **Manuscript A**.

5 CONCLUSION AND OUTLOOK

The aim of the work presented in this dissertation thesis has been to analyze biological functional principles for damage control. In this context, not only the (long-lasting) bonding, but also the debonding of (e.g., no longer functional) plant organs play a crucial role. During evolution, various concepts have evolved in this regard, three of which have been analyzed in this work by morphological, anatomical, and biomechanical methods. (i) The European mistletoe (*Viscum album*), with its structural and functional connection to the host tree, has proved to be a very suitable plant model for damage prevention analyses. Cellular and biochemical gradients at the interface, redundant anchorage through several sinkers in young mistletoes, and the continuous adaptation during joint development and competitive growth with the host are characteristics of mistletoe damage prevention making mechanical failure practically impossible in nature. (ii) *Opuntia ficus-indica* exhibits initially fragile lateral branch-branch junctions that are stabilized at young stages by growth and periderm deposition, allowing the plant to adapt its abscission concept depending on the resources invested in the organ. (iii) The branch-branch junctions of *Cylindropuntia bigelovii* exhibit fragile behavior because of the small size of the junction and the low mechanical properties of the tissues involved, allowing branch abscission to contribute to vegetative plant propagation.

Another key aspect of damage control is the ability to self-repair injured tissues. The branches of the two selected cactus species revealed good structural self-repair abilities to avoid water loss and infection by pathogens, both of which are crucial requirements for their xeromorphic lifestyles. The restoration of mechanical integrity was not observed, suggesting the principle that ‘sufficient is good enough’.

The aim of follow-up projects will be the abstraction of the investigated functional principles of damage prevention and damage management strategies by means of simulation approaches, and their translation into a shared technical language. Modern 3D-printing methods will help to transform the observed mechanisms into technical multi-material demonstrators. The adaptive and damage-resistant connection between mistletoe and its host could, for example, serve as a model for bioinspired connection techniques with redundancy strategies and adaptive gradient structures along the interface of multi-material systems with the potential for great longevity.

6 REFERENCES

ADDICOTT, F. T. (1982). *Abscission*. Berkeley: University of California Press.

ANANDAN, S., RUDOLPH, A., SPECK, T., & SPECK, O. (2018). Comparative morphological and anatomical study of self-repair in succulent cylindrical plant organs. *Flora*, *241*, 1-7.

ATHREYA, V. R. (1999). Light or presence of host trees: which is more important for the strangler fig? *Journal of Tropical Ecology*, *15*(5), 589-602.

AUKEMA, J. E. (2003). Vectors, viscin, and Viscaceae: mistletoes as parasites, mutualists, and resources. *Frontiers in Ecology and the Environment*, *1*(4), 212-219.

BADEL, E., EWERS, F. W., COCHARD, H., & TELEWSKI, F. W. (2015). Acclimation of mechanical and hydraulic functions in trees: impact of the thigmomorphogenetic process. *Frontiers in Plant Science*, *6*, 266.

BAKER, B., ZAMBRYSKI, P., STASKAWICZ, B., & DINESH-KUMAR, S. P. (1997). Signaling in plant-microbe interactions. *Science*, *276*(5313), 726-733.

BARBA, F. J., GARCIA, C., FESSARD, A., MUNEKATA, P. E., LORENZO, J. M., ABOUDIA, A., OUADIA, A., & REMIZE, F. (2020). *Opuntia ficus indica* edible parts: A food and nutritional security perspective. *Food Reviews International*, 1-23.

BARLOW, B. A., WIENS, D., WIENS, C., BUSBY, W. H., & BRIGHTON, C. (1978). Permanent translocation heterozygosity in *Viscum album* and *V. cruciatum*: sex association, balanced lethals, sex ratios. *Heredity*, *40*(1), 33-38.

BASTOLA, A. K., SOFFIATTI, P., BEHL, M., LENDLEIN, A., & ROWE, N. P. (2021). Structural performance of a climbing cactus: making the most of softness. *Journal of the Royal Society Interface*, *18*(178), 20210040.

BAUER, G., & SPECK, T. (2012). Restoration of tensile strength in bark samples of *Ficus benjamina* due to coagulation of latex during fast self-healing of fissures. *Annals of Botany*, *109*(4), 807-811.

BECKER, H. (1986). Botany of European mistletoe (*Viscum album* L.). *Oncology*, *43* (Suppl. 1), 2-7.

BEDNAREK, P., & OSBOURN, A. (2009). Plant-microbe interactions: chemical diversity in plant defense. *Science*, *324*(5928), 746-748.

BEISMANN, H., WILHELMI, H., BAILLÈRES, H., SPATZ, H. C., BOGENRIEDER, A., & SPECK, T. (2000). Brittleness of twig bases in the genus Salix: fracture mechanics and ecological relevance. *Journal of Experimental Botany*, *51*(344), 617-633.

BELL, T. L., & ADAMS, M. A. (2011). Attack on all fronts: functional relationships between aerial and root parasitic plants and their woody hosts and consequences for ecosystems. *Tree Physiology*, *31*(1), 3-15.

BENSON, L. D. (1982). *The cacti of the United States and Canada*. Stanford: Stanford University Press.

BLOCH, R. (1941). Wound healing in higher plants. *The Botanical Review*, *7*(2), 110-146.

BOBICH, E. G., & NOBEL, P. S. (2001a). Biomechanics and anatomy of cladode junctions for two *Opuntia* (Cactaceae) species and their hybrid. *American Journal of Botany*, *88*(3), 391-400.

BOBICH, E. G., & NOBEL, P. S. (2001b). Vegetative reproduction as related to biomechanics, morphology and anatomy of four cholla cactus species in the Sonoran Desert. *Annals of Botany*, *87*(4), 485-493.

BROMHAM, L., COWMAN, P. F., & LANFEAR, R. (2013). Parasitic plants have increased rates of molecular evolution across all three genomes. *BMC Evolutionary Biology*, *13*(1), 1-11.

BRYANT, J. P., PROVENZA, F. D., PASTOR, J., REICHARDT, P. B., CLAUSEN, T. P., & DU TOIT, J. T. (1991). Interactions between woody plants and browsing mammals mediated by secondary metabolites. *Annual Review of Ecology and Systematics*, *22*(1), 431-446.

BÜHRIG-POLACZEK, A., FLECK, C., SPECK, T., SCHÜLER, P., FISCHER, S. F., CALIARO, M., & THIELEN, M. (2016). Biomimetic cellular metals—using hierarchical structuring for energy absorption. *Bioinspiration & Biomimetics*, *11*(4), 045002.

BUSCH, S., SEIDEL, R., SPECK, O., & SPECK, T. (2010). Morphological aspects of self-repair of lesions caused by internal growth stresses in stems of *Aristolochia macrophylla* and *Aristolochia ringens*. *Proceedings of the Royal Society B: Biological Sciences*, *277*(1691), 2113-2120.

CAMBRIDGE UNIVERSITY PRESS (2022). Longevity. In *Cambridge Dictionary*. Retrieved April 19, 2022, from https://dictionary.cambridge.org/us/dictionary/english/longevity.

CHRISTENHUSZ, M. J., & BYNG, J. W. (2016). The number of known plants species in the world and its annual increase. *Phytotaxa*, *261*(3), 201-217

CIGNONI, P., CALLIERI, M., CORSINI, M., DELLEPIANE, M., GANOVELLI, F., & RANZUGLIA, G. (2008). Meshlab: an open-source mesh processing tool. In *Eurographics Italian chapter conference* (Vol. 2008, pp. 129-136).

CLARKE, C. R., TIMKO, M. P., YODER, J. I., AXTELL, M. J., & WESTWOOD, J. H. (2019). Molecular dialog between parasitic plants and their hosts. *Annual Review of Phytopathology*, *57*, 279-299.

COHADES, A., BRANFOOT, C., RAE, S., BOND, I., & MICHAUD, V. (2018). Progress in self-healing fiber-reinforced polymer composites. *Advanced Materials Interfaces*, *5*(17), 1800177.

CONDON, J., & KUIJT, J. (1994). Anatomy and ultrastructure of the primary endophyte of *Ileostylus micranthus* (Loranthaceae). *International Journal of Plant Sciences*, *155*(3), 350-364.

COUTANT, M. W. (1918). Wound periderm in certain cacti. *Bulletin of the Torrey Botanical Club*, *45*(9), 353-364.

CROFTS, S. B., & ANDERSON, P. S. L. (2018). The influence of cactus spine surface structure on puncture performance and anchoring ability is tuned for ecology. *Proceedings of the Royal Society B*, *285*(1891), 20182280.

DANGL, J. L., & JONES, J. D. (2001). Plant pathogens and integrated defence responses to infection. *Nature*, *411*(6839), 826-833.

DIESENDRUCK, C. E., SOTTOS, N. R., MOORE, J. S., & WHITE, S. R. (2015). Biomimetic self-healing. *Angewandte Chemie International Edition*, *54*(36), 10428-10447.

EVANS, L. S., IMSON, G. J., KIM, J. E., & KAHN-JETTER, Z. (2004). Relationships between number of stem segments on longest stems, retention of terminal stem segments andestablishment of detached terminal stem segments for 25 species of *Cylindropuntia* and *Opuntia* (Cactaceae). *Journal of the Torrey Botanical Society*, 131(3), 195-203.

GIBSON, A. C., & NOBEL, P. S. (1986). *The cactus primer*. Cambridge: Harvard University Press.

GINZBERG, I. (2008). Wound-periderm formation. In *Induced plant resistance to Herbivory* (pp. 131-146). Dordrecht: Springer.

GRAUPNER, N., LABONTE, D., HUMBURG, H., BUZKAN, T., DÖRGENS, A., KELTERER, W., & MÜSSIG, J. (2017). Functional gradients in the pericarp of the green coconut inspire asymmetric fibre-composites with improved impact strength, and preserved flexural and tensile properties. *Bioinspiration & Biomimetics*, *12*(2), 026009.

GRIL, J., JULLIEN, D., BARDET, S., & YAMAMOTO, H. (2017). Tree growth stress and related problems. *Journal of Wood Science*, *63*(5), 411-432.

GUERRERO, P. C., MAJURE, L. C., CORNEJO-ROMERO, A., & HERNÁNDEZ-HERNÁNDEZ, T. (2019). Phylogenetic relationships and evolutionary trends in the Cactus family. *Journal of Heredity*, *110*(1), 4-21.

HEIDE-JØRGENSEN, H. (2008). *Parasitic flowering plants*. Leiden: Brill.

HESSE, L., BUNK, K., LEUPOLD, J., SPECK, T., & MASSELTER, T. (2019). Structural and functional imaging of large and opaque plant specimens. *Journal of Experimental Botany*, *70*(14), 3659-3678.

HESSE, L., KAMPOWSKI, T., LEUPOLD, J., CALIARO, S., SPECK, T., & SPECK, O. (2020). Comparative analyses of the self-sealing mechanisms in leaves of *Delosperma cooperi* and *Delosperma ecklonis* (Aizoaceae). *International Journal of Molecular Sciences*, *21*(16), 5768.

HORBELT, N., EDER, M., BERTINETTI, L., FRATZL, P., & HARRINGTON, M. J. (2019). Unraveling the rapid assembly process of stiff cellulosic fibers from mistletoe berries. *Biomacromolecules*, *20*(8), 3094-3103.

HORBELT, N., FRATZL, P., & HARRINGTON, M. J. (2022). Mistletoe viscin: a hygro-and mechano-responsive cellulose-based adhesive for diverse materials applications. *PNAS Nexus*, *1*(1), pgac026.

HORN, R., ALBRECHT, S., HAASE, W., LANGER, M., SCHMEER, D., SOBEK, W., SPECK, O., & LEISTNER, P. (2019). Bio-inspiration as a concept for sustainable constructions illustrated on graded concrete. *Journal of Bionic Engineering*, *16*(4), 742-753.

JAFFE, M. J. (1973). Thigmomorphogenesis: the response of plant growth and development to mechanical stimulation. *Planta*, *114*(2), 143-157.

JOEL, D. M. (2013). Functional structure of the mature haustorium. In *Parasitic Orobanchaceae* (pp. 25-60). Berlin: Springer.

KAMINSKI, R., SPECK, T., & SPECK, O. (2017). Adaptive spatiotemporal changes in morphology, anatomy, and mechanics during the ontogeny of subshrubs with square-shaped stems. *American Journal of Botany*, *104*(8), 1157-1167.

KONRAD, W., FLUES, F., SCHMICH, F., SPECK, T., & SPECK, O. (2013). An analytic model of the self-sealing mechanism of the succulent plant *Delosperma cooperi*. *Journal of Theoretical Biology*, *336*, 96-109.

KUIJT, J. (1969). *The biology of parasitic flowering plants*. Berkeley: University of California Press.

LAMBERS, H., CHAPIN, F. S., & PONS, T. L. (2008). *Plant physiological ecology* (Vol. 2). New York: Springer.

LANGER, M., HEGGE, E., SPECK, T., & SPECK, O. (2022). Acclimation to wind loads and/or contact stimuli? A biomechanical study of peltate leaves of *Pilea peperomioides*. *Journal of Experimental Botany*, *73*(4), 1236-1252.

LANGER, M., SPECK, T., & SPECK, O. (2021). Petiole-lamina transition zone: A functionally crucial but often overlooked leaf trait. *Plants*, *10*(4), 774.

LEIMU, R., & FISCHER, M. (2008). A meta-analysis of local adaptation in plants. *PloS One*, *3*(12), e4010.

LIU, Z., MEYERS, M. A., ZHANG, Z., & RITCHIE, R. O. (2017). Functional gradients and heterogeneities in biological materials: Design principles, functions, and bioinspired applications. *Progress in Materials Science*, *88*, 467-498.

LOSNER-GOSHEN, D., PORTNOY, V. H., MAYER, A. M., & JOEL, D. M. (1998). Pectolytic activity by the haustorium of the parasitic Plant *Orobanche* L. (Orobanchaceae) in host roots. *Annals of Botany*, *81*(2), 319-326.

LUCAS, S. S., VON TAPAVICZA, M., SCHMIDT, A. M., BERTLING, J., & NELLESEN, A. (2016). Study of quantification methods in self-healing ceramics, polymers and concrete: A route towards standardization. *Journal of Intelligent Material Systems and Structures*, *27*(19), 2577-2598.

MAJURE, L. C., PUENTE, R., GRIFFITH, M. P., JUDD, W. S., SOLTIS, P. S., & SOLTIS, D. E. (2012). Phylogeny of *Opuntia* s.s. (Cactaceae): clade delineation, geographic origins, and reticulate evolution. *American Journal of Botany*, *99*(5), 847-864.

MASUMOTO, N., SUZUKI, Y., CUI, S., WAKAZAKI, M., SATO, M., KUMAISHI, K., ... & YOSHIDA, S. (2021). Three-dimensional reconstructions of haustoria in two parasitic plant species in the Orobanchaceae. *Plant Physiology*, *185*(4), 1429-1442.

MAUSETH, J. D. (2006). Structure–function relationships in highly modified shoots of Cactaceae. *Annals of Botany*, *98*(5), 901-926.

MAUSETH, J. D., & REZAEI, K. (2013). Morphogenesis in the parasitic plant *Viscum minimum* (Viscaceae) is highly altered, having apical meristems but lacking roots, stems, and leaves. *International Journal of Plant Sciences*, *174*(5), 791-801.

MOREL, S., SCHMITTBUHL, J., LÓPEZ, J. M., & VALENTIN, G. (1998). Anomalous roughening of wood fractured surfaces. *Physical Review E*, *58*(6), 6999.

MORRIS, J. L., PUTTICK, M. N., CLARK, J. W., EDWARDS, D., KENRICK, P., PRESSEL, S., WELLMAN, C. H., YANG, Z., SCHNEIDER, H., & DONOGHUE, P. C. (2018). The timescale of early land plant evolution. *Proceedings of the National Academy of Sciences*, *115*(10), E2274-E2283.

NAGAR, R., SINGH, M., & SANWAL, G. G. (1984). Cell wall degrading enzymes in *Cuscuta reflexa* and its hosts. *Journal of Experimental Botany*, *35*(8), 1104-1112.

NAUMANN, J., SALOMO, K., DER, J. P., WAFULA, E. K., BOLIN, J. F., MAASS, E., ... & WANKE, S. (2013). Single-copy nuclear genes place haustorial Hydnoraceae within Piperales and reveal a Cretaceous origin of multiple parasitic angiosperm lineages. *PLoS One*, *8*(11), e79204.

NICKRENT, D. L. (2020). Parasitic angiosperms: how often and how many? *Taxon*, *69*(1), 5-27.

NIERHAUS-WUNDERWALD, D., & LAWRENZ, P. (1997). *Zur Biologie der Mistel*. Birmensdorf: Bibliothek WSL.

NIKLAS, K. J. (1992). *Plant biomechanics: an engineering approach to plant form and function*. Chicago: University of Chicago press.

NIKLAS, K. J. (1994). *Plant allometry: the scaling of form and process*. Chicago: University of Chicago Press.

NIKOLOV, L. A., TOMLINSON, P. B., MANICKAM, S., ENDRESS, P. K., KRAMER, E. M., & DAVIS, C. C. (2014). Holoparasitic Rafflesiaceae possess the most reduced endophytes and yet give rise to the world's largest flowers. *Annals of Botany*, *114*(2), 233-242.

NOBEL, P. S. (2002). *Cacti: biology and uses*. Berkeley: University of California Press.

NOBEL, P. S., & MEYER, R. W. (1991). Biomechanics of cladodes and cladode-cladode junctions for *Opuntia ficus-indica* (Cactaceae). *American Journal of Botany*, *78*(9), 1252-1259.

OUYANG, Y., ZHANG, X., CHEN, Y., TEIXEIRA DA SILVA, J. A., & MA, G. (2016). Growth, photosynthesis and haustorial development of semiparasitic *Santalum album* L. penetrating into roots of three hosts: a comparative study. *Trees*, *30*(1), 317-328.

PAN, B., QIAN, K., XIE, H., & ASUNDI, A. (2009). Two-dimensional digital image correlation for in-plane displacement and strain measurement: a review. *Measurement Science and Technology*, *20*(6), 062001.

PARKER, C. (2012). Parasitic weeds: a world challenge. *Weed Science*, *60*(2), 269-276.

PAUL-VICTOR, C., DALLE VACCHE, S., SORDO, F., FINK, S., SPECK, T., MICHAUD, V., & SPECK, O. (2017). Effect of mechanical damage and wound healing on the viscoelastic properties of stems of flax cultivars (*Linum usitatissimum* L. cv. Eden and cv. Drakkar). *PLoS One*, *12*(10), e0185958.

PIERANTONI, M., BRUMFELD, V., ADDADI, L., & WEINER, S. (2019). A 3D study of the relationship between leaf vein structure and mechanical function. *Acta Biomaterialia*, *88*, 111-119.

PIIRTO, D. D., CREWS, D. L., & TROXELL, H. E. (1974). The effects of dwarf mistletoe on the wood properties of lodgepole pine. *Wood and Fiber Science*, *6*(1), 26-35.

RAMPF, M., SPECK, O., SPECK, T., & LUCHSINGER, R. H. (2013). Investigation of a fast mechanical self-repair mechanism for inflatable structures. *International Journal of Engineering Science*, *63*, 61-70.

REBMAN, J. P., & PINKAVA, D. J. (2001). *Opuntia* cacti of North America: an overview. *Florida Entomologist*, 474-483.

ROWE, N., ISNARD, S., & SPECK, T. (2004). Diversity of mechanical architectures in climbing plants: an evolutionary perspective. *Journal of Plant Growth Regulation*, *23*(2), 108-128.

ROWE, N. P., & SPECK, T. (2015). Stem biomechanics, strength of attachment, and developmental plasticity of vines and lianas. *Ecology of Lianas*, 323-341.

SCHINDELIN, J., ARGANDA-CARRERAS, I., FRISE, E., KAYNIG, V., LONGAIR, M., PIETZSCH, T., ... & CARDONA, A. (2012). Fiji: an open-source platform for biological-image analysis. *Nature Methods*, *9*(7), 676-682.

SCHMIER, S., HOSODA, N., & SPECK, T. (2020a). Hierarchical structure of the *Cocos nucifera* (coconut) endocarp: Functional morphology and its influence on fracture toughness. *Molecules*, *25*(1), 223.

SCHMIER, S., JENTZSCH, M., SPECK, T., & THIELEN, M. (2020b). Fracture mechanics of the endocarp of *Cocos nucifera*. *Materials & Design*, *195*, 108944.

SCHOLES, J. D., & PRESS, M. C. (2008). *Striga* infestation of cereal crops–an unsolved problem in resource limited agriculture. *Current Opinion in Plant Biology*, *11*(2), 180-186.

SCHWAGER, H., MASSELTER, T., SPECK, T., & NEINHUIS, C. (2013). Functional morphology and biomechanics of branch–stem junctions in columnar cacti. *Proceedings of the Royal Society B: Biological Sciences*, *280*(1772), 20132244.

SEXTON, R., & ROBERTS, J. A. (1982). Cell biology of abscission. *Annual Review of Plant Physiology*, *33*(1), 133-162.

SHINGLETON, A. (2010). Allometry: the study of biological scaling. *Nature Education Knowledge*, *3*(10), 2.

SHOWLER, K. (1974). Raising mistletoe (*Viscum album*) from seed. *Journal of the Royal Horticultural Society*, 99, 30–37.

SHTEIN, I., KOYFMAN, A., ESHEL, A., & BAR-ON, B. (2019). Autotomy in plants: organ sacrifice in *Oxalis* leaves. *Journal of the Royal Society Interface*, *16*(151), 20180737.

SMITH, P. L., & GLEDHILL, D. (1983). Anatomy of the endophyte of *Viscum album* L. (Loranthaceae). *Botanical Journal of the Linnean Society*, *87*(1), 29-53.

SPECK, O., SCHLECHTENDAHL, M., BORM, F., KAMPOWSKI, T., & SPECK, T. (2018). Humidity-dependent wound sealing in succulent leaves of *Delosperma cooperi*–An adaptation to seasonal drought stress. *Beilstein Journal of Nanotechnology*, *9*(1), 175-186.

SPECK, O., SCHMAUDER, K., SPECK, T., & PAUL-VICTOR, C. (2020). Wound reactions in stems of *Leonurus cardiaca*: A morphological, anatomical, and biomechanical study. *Botany*, *98*(1), 81-89.

SPECK, O., SPECK, D., HORN, R., GANTNER, J., & SEDLBAUER, K. P. (2017). Biomimetic bio-inspired biomorph sustainable? An attempt to classify and clarify biology-derived technical developments. *Bioinspiration & Biomimetics*, *12*(1), 011004.

SPECK, O., & SPECK, T. (2019). An overview of bioinspired and biomimetic self-repairing materials. *Biomimetics*, *4*(1), 26.

STANTON, S., HONNAY, O., JACQUEMYN, H., & ROLDÁN-RUIZ, I. (2009). A comparison of the population genetic structure of parasitic *Viscum album* from two landscapes differing in degree of fragmentation. *Plant Systematics and Evolution*, *281*(1), 161-169.

STEINBRECHER, T., DANNINGER, E., HARDER, D., SPECK, T., KRAFT, O., & SCHWAIGER, R. (2010). Quantifying the attachment strength of climbing plants: a new approach. *Acta Biomaterialia*, 6(4), 1497-1504.

STUDART, A. R., LIBANORI, R., & ERB, R. M. (2014). Functional gradients in biological composites. *Bio-and Bioinspired Nanomaterials*, 335-368.

SU, H. J., HU, J. M., ANDERSON, F. E., DER, J. P., & NICKRENT, D. L. (2015). Phylogenetic relationships of Santalales with insights into the origins of holoparasitic Balanophoraceae. *Taxon*, *64*(3), 491-506.

TEIXEIRA-COSTA, L. (2021). A living bridge between two enemies: haustorium structure and evolution across parasitic flowering plants. *Brazilian Journal of Botany*, *44*(1), 165-178.

TEIXEIRA-COSTA, L., & CECCANTINI, G. C. (2016). Aligning microtomography analysis with traditional anatomy for a 3D understanding of the host-parasite interface–*Phoradendron* spp. case study. *Frontiers in Plant Science*, *7*, 1340.

TEIXEIRA-COSTA, L., & DAVIS, C. C. (2021). Life history, diversity, and distribution in parasitic flowering plants. *Plant Physiology*, *187*(1), 32-51.

TEIXEIRA-COSTA, L., DAVIS, C. C., & CECCANTINI, G. (2021). Striking developmental convergence in angiosperm endoparasites. *American Journal of Botany*, *108*(5), 756-768.

TELEWSKI, F. W. (2021). Mechanosensing and plant growth regulators elicited during the thigmomorphogenetic response. *Frontiers in Forests and Global Change*, *3*, 147.

TELEWSKI, F. W., & JAFFE, M. J. (1986). Thigmomorphogenesis: anatomical, morphological and mechanical analysis of genetically different sibs of *Pinus taeda* in response to mechanical perturbation. *Physiologia Plantarum*, *66*(2), 219-226.

TĚŠITEL, J. (2016). Functional biology of parasitic plants: a review. *Plant Ecology and Evolution*, *149*(1), 5-20.

THODAY, D. (1951). The haustorial system of *Viscum album*. *Journal of Experimental Botany*, *2*(1), 1-19.

TWYFORD, A. D. (2018). Parasitic plants. *Current Biology*, *28*(16), R857-R859.

UNITED NATIONS (2016). Transforming our World: The 2030 Agenda for Sustainable Development. Retrieved April 19, 2022, from https://sustainabledevelopment.un.org/content/documents/21252030%20Agenda%20for%20Sustainable%20Development%20web.pdf

VALLAURI, D. R., ARONSON, J., & BARBERO, M. (2002). An analysis of forest restoration 120 years after reforestation on badlands in the Southwestern Alps. *Restoration Ecology*, *10*(1), 16-26.

VARGA, I., POCZAI, P., TIBORCZ, V., ARANYI, N. R., BALTAZÁR, T., BARTHA, D., PEJCHAL, M., & HYVÖNEN, J. (2014). Changes in the distribution of European mistletoe (*Viscum album*) in Hungary during the last hundred years. *Folia Geobotanica*, *49*(4), 559-577.

VOGEL, S. (1989). Drag and reconfiguration of broad leaves in high winds. *Journal of Experimental Botany*, *40*(8), 941-948.

WATSON, D. M. (2001). Mistletoe—a keystone resource in forests and woodlands worldwide. *Annual Review of Ecology and Systematics*, *32*(1), 219-249.

WATSON, D. M., COOK, M., & FADINI, R. F. (2020). Towards best-practice management of mistletoes in horticulture. *Botany*, *98*(9), 489-498.

WEGST, U. G., BAI, H., SAIZ, E., TOMSIA, A. P., & RITCHIE, R. O. (2015). Bioinspired structural materials. *Nature Materials*, *14*(1), 23-36.

WESTWOOD, J. H., YODER, J. I., TIMKO, M. P., & DEPAMPHILIS, C. W. (2010). The evolution of parasitism in plants. *Trends in Plant Science*, *15*(4), 227-235.

WIECZOREK, G. F. (2002). Catastrophic rockfalls and rockslides in the Sierra Nevada, USA. In *Catastrophic landslides: effects, occurrence, and mechanisms* (Vol. 15, pp. 165-190). Boulder: Geological Society of America Reviews in Engineering Geology.

WIENS, D., NICKRENT, D. L., SHAW, C. G., HAWKSWORTH, F. G., HENNON, P. E., & KING, E. J. (1996). Embryonic and host-associated skewed adult sex ratios in dwarf mistletoe. *Heredity*, *77*(1), 55-63.

YANG, Y. Y., & KIM, J. G. (2016). The optimal balance between sexual and asexual reproduction in variable environments: a systematic review. *Journal of Ecology and Environment*, 40(1), 1-18.

YOSHIDA, S., CUI, S., ICHIHASHI, Y., & SHIRASU, K. (2016). The haustorium, a specialized invasive organ in parasitic plants. *Annual Review of Plant Biology*, *67*, 643-667.

ZOTZ, G., & HIETZ, P. (2001). The physiological ecology of vascular epiphytes: current knowledge, open questions. *Journal of Experimental Botany*, *52*(364), 2067-2078.

ZUBER, D. (2004). Biological flora of central Europe: *Viscum album* L. *Flora-Morphology, Distribution, Functional Ecology of Plants*, *199*(3), 181-203.

Part II

ARTICLES AND MANUSCRIPTS

Article A

Mylo, M. D., Krüger, F., Speck, T., & Speck, O. (2020). Self-repair in cacti branches: Comparative analyses of their morphology, anatomy, and biomechanics. *International Journal of Molecular Sciences*, *21*(13), 4630.

Article B

Speck, O., Langer, M., & Mylo, M. D. (2022). Plant-inspired damage control–An inspiration for sustainable solutions in the Anthropocene. *The Anthropocene Review*, *9*(2), 220-236.

Article C

Mylo, M. D., Hofmann, M., Delp, A., Scholz, R., Walther, F., Speck, T., & Speck, O. (2021). Advances on the visualization of the internal structures of the European mistletoe: 3D reconstruction using microtomography. *Frontiers in Plant Science*, *12*, 715711.

Article D

Mylo, M. D., Hesse, L., Masselter, T., Leupold, J., Drozella, K., Speck, T., & Speck, O. (2021). Morphology and anatomy of branch–branch junctions in *Opuntia ficus-indica* and *Cylindropuntia bigelovii*: a comparative study supported by mechanical tissue quantification. *Plants*, *10*(11), 2313.

Article E

Mylo, M. D., Hofmann, M., Balle, F., Beisel, S., Speck, T., & Speck, O. (2022). Biomechanics of the parasite–host interaction of the European mistletoe. *Journal of Experimental Botany*, *73*(4), 1204-1221.

Manuscript A (Meanwhile fully published)

Mylo, M., Hoppe, A., Pastewka, L., Speck, T., & Speck, O. (2022). Elastic property and fracture mechanics of lateral branch-branch junctions in cacti: A case study of *Opuntia ficus-indica* and *Cylindropuntia bigelovii*. *Frontiers in plant science*, *13*, 950860.

Part III
List of Publications

Peer-reviewed articles

***Mylo MD, Hoppe A, Pastewka L, Speck T & Speck O. 2022.** Elastic property and fracture mechanics of lateral branch-branch junctions in cacti: A case study of *Opuntia ficus-indica* and *Cylindropuntia bigelovii*. *Frontiers in plant science*, *13*, 950860.

***Hone T, Mylo MD, Speck O & Taylor D. 2022.** Investigating defect tolerance and failure mechanisms of three plant stems with different cross-sectional tissue patterns. (submitted).

***Ludwig F, Rahman MA, Mylo MD, Speck O, Fleckenstein C, Shu Q & Speck T. 2022.** Joining trees for future cities: a long-term inosculation study for living architecture. (submitted).

***Mylo MD, Hofmann M, Balle F, Beisel S, Speck T & Speck O. 2022**. Biomechanics of the Parasite-Host Interaction of the European Mistletoe. *Journal of Experimental Botany*, 73(4): 1204-1221. doi: 10.1093/jxb/erab518

***Mylo MD, Hesse L, Masselter T, Leupold J, Drozella K, Speck T & Speck O. 2021**. Morphology and Anatomy of Branch–Branch Junctions in *Opuntia ficus-indica* and *Cylindropuntia bigelovii*: A Comparative Study Supported by Mechanical Tissue Quantification. *Plants*, 10(11): 2313. doi: 10.3390/plants10112313

***Mylo MD, Hofmann M, Delp A, Scholz R, Walther F, Speck T & Speck O. 2021.** Advances on the visualization of the internal structures of the European mistletoe: 3D reconstruction using microtomography. *Frontiers in Plant Science*, 12: 715711. doi: 10.3389/fpls.2021.715711

***Speck O, Langer M & Mylo MD. 2021.** Plant-inspired damage control—an inspiration for sustainable solutions in the Anthropocene. *The Anthropocene Review*, 20530196211018489. doi: 10.1177/20530196211018489

***Hone T, Mylo MD, Speck O, Speck T & Taylor D. 2021.** Failure mechanisms and bending strength of *Fuchsia magellanica* var. *gracilis* stems. *Journal of the Royal Society Interface,* 18(175): 20201023. doi: 10.1098/rsif.2020.1023

Yin K, Mylo MD, Speck T & Wegst UGK. 2020. 2D and 3D graphical datasets for bamboo-inspired tubular scaffolds with functional gradients: micrographs and tomograms. *Data in Brief*, 31: 105870. doi: 10.1016/j.dib.2020.105870

Sachse R, Westermeier AS, Mylo MD, Nadasdi J, Bischoff M, Speck T & Poppinga S. 2020. Snapping mechanics of the Venus flytrap (*Dionaea muscipula*). *Proceedings of the National Academy of Sciences*, 11727: 16035-16042. doi: 10.1073/pnas.2002707117

Yin K, Mylo MD, Speck T & Wegst UGK. 2020. Bamboo-inspired tubular scaffolds with functional gradients. *Journal of the Mechanical Behavior of Biomedical Materials*, 110: 103826. doi: 10.1016/j.jmbbm.2020.103826

Correa D, Poppinga S, Mylo MD, Westermeier AS, Bruchmann B, Menges A & Speck T. 2019. 4D pine scale: Biomimetic 4D printed autonomous scale and flap structures capable of multi-phase movement. *Philosophical Transactions of the Royal Society A*, 378(2167): 20190445. doi: 10.1098/rsta.2019.0445

***Mylo MD, Krüger F, Speck T & Speck O. 2020.** Self-repair in cacti branches: Comparative analyses of their morphology, anatomy, and biomechanics. *International Journal of Molecular Sciences*, 21(13): 4630. doi: 10.3390/ijms21134630

Ferger K, Hackbarth M, Mylo MD, Müller C & Zentgraf K. 2019. Measuring temporal and spatial accuracy in trampolining. *Sports Engineering*, 22(3-4): 18. doi: 10.1007/s12283-019-0310-9

Esser F, Scherag FD, Poppinga S, Westermeier A, Mylo MD, Kampowski T, Bold G, Rühe J & Speck T. 2019. Adaptive biomimetic actuator systems reacting to various stimuli by and combining two biological snap-trap mechanics. In *Conference on Biomimetic and Biohybrid Systems* (pp. 114-121). Springer, Cham. doi: 10.1007/978-3-030-24741-6_10

Kampowski T, Mylo MD, Poppinga S & Speck T. 2018. How water availability influences morphological and biomechanical properties in the one-leaf plant *Monophyllaea horsfieldii. Royal Society open Science*, 5(1): 171076. doi: 10.1098/rsos.171076

Publications marked with an asterisk (*****) are in the direct or in the broader context of the topic of this thesis.

Conference contributions

Mylo MD, Hofmann M, Beisel S, Balle F, Speck T & Speck O. 2022. The European mistletoe and its multi-functional connection to the host: a source of inspiration for bioinspired joining techniques. 6th International School and Conference on Biological Materials Science BioINSP 2022 (virtual). (21.-24.03.2022; **keynote talk**)

Mylo MD, Hofmann M, Speck T & Speck O. 2021. Connecting two biological materials systems on the example of the European mistletoe. *liv*MatS retreat 2021 (virtual). (17.-19.11.2021; **poster**)

Mylo MD, Hoppe A, Pastewka L, Speck T & Speck O. 2021. Abscission in biological materials systems - A case study on cacti junctions. *liv*MatS retreat 2021 (virtual, tandem talk). (17.-19.11.2021; **talk**)

Mylo MD, Hofmann M, Beisel S, Balle F, Speck T & Speck O. 2021. The structural and functional connection of two biological, fibre-reinforced composites: a case study on the European mistletoe. FIT colloquium 2021 (virtual). (12.-12.10.2021; **talk**)

Mylo MD, Hofmann M, Beisel S, Balle F, Speck T & Speck O. 2021. Staying in touch - The European Mistletoe (*Viscum album*) and its multifunctional connection to the host. EUROMAT conference (virtual). (13.-17.09.2021; **talk**)

Mylo MD, Hesse L, Masselter T, Leupold J, Drozella K, Speck T & Speck O. 2021. Why the jumping cholla jumps – a comparative study on the branch-branch junction stability in Opuntioideae. SEB Annual Main Meeting (virtual). (29.06.-08.07.2021; **talk**)

Mylo MD, Speck T & Speck O. 2020. Damage management in plants. *liv*MatS SAB-meeting (virtual). (18.11.2020; **talk**)

Yin K, Mylo MD, Shubitidze F, Speck & Wegst UGK. 2019. Bamboo-inspired porous tubes: Permeability, flow, and water purification. 8th International Conference on Mechanics of Biomaterials and Tissues, Hawaii, United States. (15-19.12.2019; **poster**)

Mylo MD, Krüger F, Speck T & Speck O. 2019. Biomechanical and morphological characterization of intact, damaged and healed branches comparing two species of Opuntioideae. 4. Bocholter Bionik-Workshop, Bocholt, Germany. (14.11.2019; **poster**)

Mylo MD, Speck T & Speck O. 2019. Damage control analyses in two species of the Opuntioideae (Cactaceae). *liv*MatS retreat, Müllheim, Germany. (13.-15.11.2019; **poster**)

Mylo MD, Speck T & Speck O. 2019. Comparative analyses of damage control in two species of the Opuntioideae (Cactaceae). *liv*MatS Kickoff meeting, Freiburg, Germany. (26.-27.09.2019; **poster**)

Mylo MD, Westermeier AS, Poppinga S & Speck T. 2019. Assessment of a digital image correlation-based methodology for quantitative full-field 3D plant movement and deformation analyses. SEB Annual Main Meeting, Seville, Spain. (02.-05.07.2019; **talk**)

Mylo MD, Krüger F, Speck T & Speck O. 2019. Biomechanical and morphological-anatomical characterization of intact, damaged and healed branches comparing two species of Opuntioideae. SEB Annual Main Meeting, Seville, Spain. (02.-05.07.2019; **short talk and poster**)

Yin K, Mylo MD, Speck T & Wegst U. 2019. Bamboo-inspired Tubular Scaffolds with Functional Gradients. MRS Spring Meeting & Exhibit in Phoenix, Arizona, United States. (22.-26.4.2019; **talk**)

Mylo MD, Westermeier AS, Poppinga & Speck T. 2019. Establishment of a methodology for full-field 3D displacement and deformation analyses of plants and (bio-inspired) technical materials systems and structures. In: Kesel, A.B. & Zehren, D. (eds.) *Bionik: Patente aus der Natur (GTBB) Tagungsband 9. Bremer Bionik-Kongress 2018*, 211–216. ISBN: 978300061443 (**Conference proceeding**)

Mylo MD, Westermeier AS, Poppinga S & Speck T. 2018. 3D full-field displacement and deformation measurements on plant structures using stereo-camera setups and DIC. Biomimetics Congress at the City University of Applied Sciences, Bremen, Germany. (26.-27.10.2016, **short talk and poster**)

Kampowski T, Mylo MD, Demandt S, Poppinga S & Speck T. 2018. Herbaceous shape memory material systems: Structural and biomechanical adaptations to desiccation in the resurrection plant *Ramonda myconi*. Plant Biomechanics Conference, Montreal, Canada. (09.-14.08.2018; **poster**)

Annual reports

Mylo MD, Hoppe A, Pastewka L, Speck T & Speck O. 2022. Simulation of cactus junctions based on geometric and biomechanical analyses of the biological role models. In: Freiburg Center for Interactive Materials and Bioinspired Technologies (FIT) Report 2021, 40-41. ISBN: 987-3-946018-07-0

Mylo MD, Krüger F, Speck T & Speck O. 2021. Damage management in cacti. In: Freiburg Center for Interactive Materials and Bioinspired Technologies (FIT) Report 2020, 37-38. ISBN: 987-3-946018-06-3

Mylo MD, Krüger F, Speck T & Speck O. 2020. Self-healing in cacti branches: a morphological, anatomical and biomechanical analysis. In: Freiburg Center for Interactive Materials and Bioinspired Technologies (FIT) Report 2019, 43-44. ISBN: 987-3-946018-05-6

Westermeier AS, Mylo MD, Poppinga S, Masselter T & Speck T. 2019. Full-field 3D deformation and displacement analyses on plant surfaces. In: Freiburg Center for Interactive Materials and Bioinspired Technologies (FIT) Report 2018, 39-41. ISBN: 987-3-946018-06-3